Received: 3 August 2020 | Revised: 8 October 2020 | Accepted: 20 October 2020

DOI: 10.1002/wsbm.1514

ADVANCED REVIEW

WIREs MECHANISMS OF DISEASE WILEY

Tools for computational analysis of moving boundary problems in cellular mechanobiology

Kathleen T. DiNapoli[1] | **Douglas N. Robinson**[1] | **Pablo A. Iglesias**[1,2]

[1]Department of Cell Biology, Johns Hopkins School of Medicine, Baltimore, Maryland

[2]Department of Electrical & Computer Engineering, Johns Hopkins University, Baltimore, Maryland

Correspondence
Pablo A. Iglesias, Department of Electrical and Computer Engineering, Johns Hopkins University, 3400 North Charles Street, Baltimore, MD 21218.
Email: pi@jhu.edu

Funding information
National Institutes of Health/National Institute of General Medical Sciences, Grant/Award Number: GM66817; Defense Advanced Research Projects Agency, Grant/Award Number: HR0011-16-C-0139

Abstract

A cell's ability to change shape is one of the most fundamental biological processes and is essential for maintaining healthy organisms. When the ability to control shape goes awry, it often results in a diseased system. As such, it is important to understand the mechanisms that allow a cell to sense and respond to its environment so as to maintain cellular shape homeostasis. Because of the inherent complexity of the system, computational models that are based on sound theoretical understanding of the biochemistry and biomechanics and that use experimentally measured parameters are an essential tool. These models involve an inherent feedback, whereby shape is determined by the action of regulatory signals whose spatial distribution depends on the shape. To carry out computational simulations of these moving boundary problems requires special computational techniques. A variety of alternative approaches, depending on the type and scale of question being asked, have been used to simulate various biological processes, including cell motility, division, mechanosensation, and cell engulfment. In general, these models consider the forces that act on the system (both internally generated, or externally imposed) and the mechanical properties of the cell that resist these forces. Moving forward, making these techniques more accessible to the non-expert will help improve interdisciplinary research thereby providing new insight into important biological processes that affect human health.

This article is categorized under:

Cancer > Cancer>Computational Models

Cancer > Cancer>Molecular and Cellular Physiology

KEYWORDS

biomechanics, chemotaxis, computational modeling, cytokinesis, moving boundary

1 | INTRODUCTION

One of the most remarkable aspects of cells is their ability to alter shape. These changes enable them to carry out numerous physiological tasks. Changes in cell morphology start at the very beginning of a cell's existence: it is through the series of dramatic cell shape changes seen in cytokinesis that mother cells divide, leading to newly formed daughter cells. Changes in morphology will continue to be crucial to these cells' survival. For example, acquiring nutrients may first require that cells migrate. This motility involves numerous but also quite distinct changes in cell morphology, from the broad lamellipodia that allows keratocytes to glide over epithelial surfaces, to the more focused pseudopods used in

amoeboid locomotion, to the thin filopodia used by fibroblasts to direct migration and wound closure. Once these cells reach their target, cellular shape changes are required to ingest it and break it down as a nutrient source.

In the cancer scenario, altered cell mechanical properties along with altered mechanosensitivity are emerging as hallmarks of the disease (Cross, Jin, Rao, & Gimzewski, 2007; Surcel et al., 2019; Surcel & Robinson, 2019). Solid tumors are frequently described as being stiffer than the surrounding tissue, but as soon as the cancer cells disseminate, initiating the metastasis process, they often become more deformable, perhaps potentiating the ability of the cells to survive in the ever-changing mechanical landscape (Cross et al., 2007; Nguyen et al., 2016; Remmerbach et al., 2009; Swaminathan et al., 2011). Then, circulating tumor cells experience ongoing shear stresses in the vasculature, and more deformable cells are better able to survive this environment (Xin et al., 2019). Within the solid tumor, evidence of mechanical heterogeneity may be further discerned from the relatively high prevalence of entosis (a.k.a. cell-in-cell or cell cannibalism), the process by which a more deformable cell engulfs a neighboring stiffer cell (Overholtzer et al., 2007; Sun et al., 2014). A recent study found that presence of entosis correlated strongly with poor patient outcomes of pancreatic cancer (Hayashi et al., 2020). These observations collectively suggest that the increased mechanical heterogeneity in the tumor could be a predictor of poor patient survival.

Though cell shape has typically been considered as the result of forces resulting from the action of biochemical signaling, it is also known that the influence flows in the other direction, closing feedback loops between mechanical and biochemical signals (Hannezo & Heisenberg, 2019; Kothari, Johnson, Sandone, Iglesias, & Robinson, 2019). Importantly, cell shape alone can dictate the behavior of a biological system (Meyers, Craig, & Odde, 2006; Rangamani et al., 2013). Moreover, there is a growing appreciation that extracellular forces can also alter inherently biochemical pathways, a process known as *mechanosensation* (Bellas & Chen, 2014; Mohammadi & Sahai, 2018; Rodrigues, Kosaric, Bonham, & Gurtner, 2019). Mechanical stimuli from external forces change the internal signaling and ultimately result in significant cell shape changes, while simultaneously altering the biochemical pathways and signaling for modulation of internal biophysical pathways.

Given the fundamental role of mechanics and cell morphogenesis in the function of healthy and disease scenarios, in this review we present the current status of mathematical modeling of cell shape change and mechanics. We consider the critical mechanical elements, the major mathematical frameworks for modeling these cellular systems, and model cell processes, including cell migration, cytokinesis, mechanosensation, and mechanotransduction and cell-in-cell events including phagocytosis and entosis.

2 | MECHANICAL DESCRIPTION OF CELLS

The shape of the cell is an inherently physical property. Physical forces on the cell are counteracted by the mechanical resistances that oppose them. These forces arise from the environment but can also be produced by the cell itself as a result of the action of biochemical pathways. Assisting in the cells' ability to maintain its deformed shape are adhesion molecules that can attach to a surface to counteract retraction forces from the inherent physical properties of the cell cortex.

Mechanical models of cells fall roughly into two classes depending on whether components are modeled using discrete elements or a continuum approach. In both cases, the assumption is that the motion of cells and their components act in a low Reynolds number regime which allows all inertial forces to be ignored (Berg, 1993). To understand the evolution of the cell we consider both the forces that deform the cell as well as the mechanics that resist these forces.

2.1 | The mechanics of viscoelastic cells: discrete elements

Cells have typically been modeled as viscoelastic materials, having both the elastic properties of solids and the viscous properties of a liquid. For relatively small forces and deformations, elastic objects obey Hooke's law, in which the force (F) and deformation (x) are proportional: $F = kx$. This assumes that the deformation is measured from a resting position. Though it is customary to write Hooke's law as above, it must be understood that the spring's force is a restoring one as it opposes the displacement that is induced by an external force. If we consider a spring of resting length L strewn between two points in space, x_i and x_j, then

$$F_{ij} = -k\underbrace{\left(\frac{\left\|x_i - x_j\right\|}{L} - 1\right)}_{\epsilon}\frac{x_i - x_j}{\left\|x_i - x_j\right\|}$$

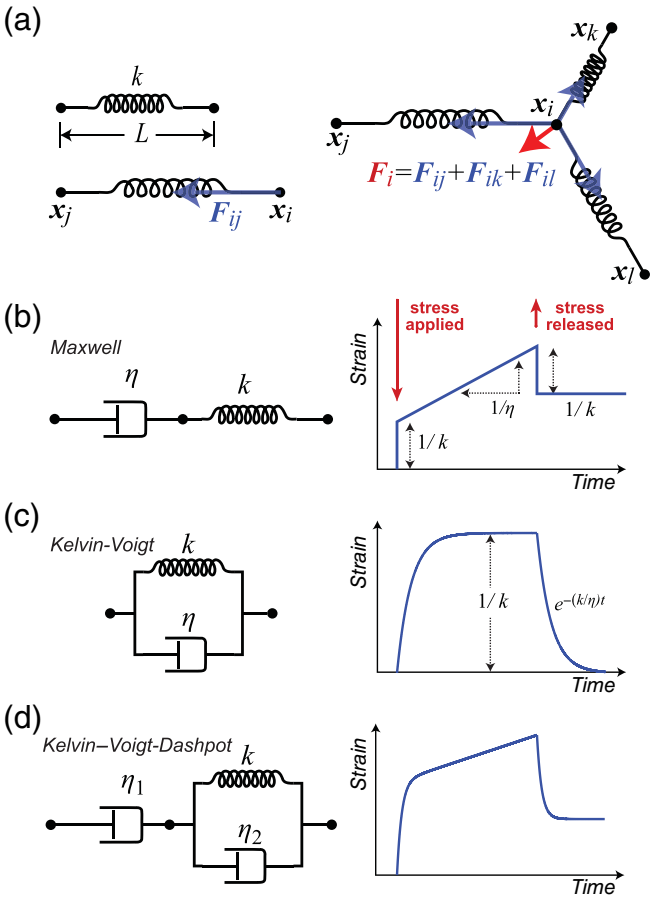

FIGURE 1 Discrete mechanical models of cells. (a) The spring joining two masses at x_i and x_j induces a force if the distance between the two points is different than the resting length L. Whereas the magnitude of the force is proportional to the displacement away from the spring's resting point, the direction of the force is along the vector between the two points acting away from the deviation. Thus, when stretched, the force acts to move the two masses towards each other. The force shown, F_{ij} is the force on mass at x_i; there is an equivalent force on this mass pointing towards x_i. On the right is shown the net force (red) of the three springs that act on the mass at x_i. (b) A Maxwell mechanical element consists of a series connection of a spring and viscous damper. The graph on the right shows the strain when a constant force is first applied and then removed. Whereas the elastic component is responsible for the two instant jumps, the continuous lengthening is due to the viscous damper. (c) In a Kelvin–Voigt element, the damper and spring are in parallel. On the right is the corresponding strain. Note that in this case there are no instant jumps and there is a maximum strain. (d). Mechanical model combining a Kelvin–Voigt element in series with a second viscous damper, and its corresponding strain

denotes the force vector acting on the object at position x_i (Figure 1a). Note how the term ϵ in the bracket denotes a normalized deviation away from the resting length. This non-dimensional quantity is the *strain*. The term at the end denotes the directionality of the vector force.

Viscous elements obey similar equations, but in this case the magnitude of the force is proportional to the strain *rate*, the change in strain over time: $F = \eta\dot{x}$. Viscoelastic materials share some of these properties. If the same force acts on both the elastic and viscous elements—for example, the effect of a micropipette aspirating a cell—then the deformation is the sum of the two individual components. In this *Maxwell* model (Figure 1b), the total deformation follows $\eta\dot{F} + \eta kF = k\dot{x}$. A common alternative for capturing viscoelastic behavior is the *Kelvin–Voigt* model (Figure 1c), which assumes that the force is shared by the two elements. In this case, the viscous and elastic deformations are the same and obey: $F = kx + \eta\dot{x}$. Other possibilities exist but are just extensions of these two basic models. For example, experiments using *Dictyostelium* cells showed that the ingression into an aspirating micropipette followed the model shown in Figure 1d in which a Kelvin–Voigt model is in series with a purely viscous damper (Yang et al., 2008). In this case, the force and displacement are related by

$$(\eta_1 + \eta_2)\dot{F} + k_2 F = \eta_1\eta_2\ddot{x} + \eta_2 k\dot{x}. \quad (1)$$

2.2 | Continuum description of cell

The description given above is appropriate for characterizing deformations of discrete particles held together by mechanical elements. When considering a continuum description of an object, the analysis is similar but must account for the fact there are no discrete elements.

To illustrate the basic ideas, we consider a tensile stress acting along the x-dimension perpendicular to the face of an object (Figure 2a). This causes a strain in the x-direction. In this case we write the stress–strain relationship as

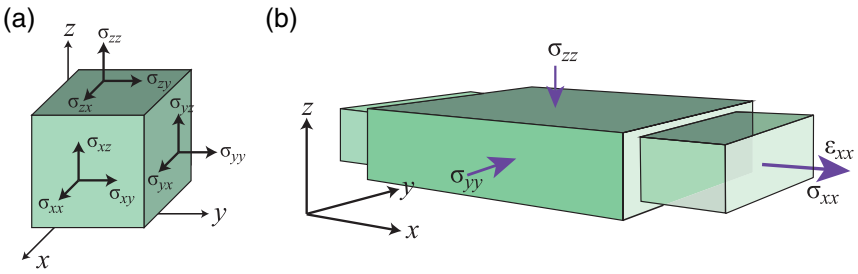

FIGURE 2 Continuum description of mechanics. (a) Coordinates for a three-dimensional continuum representation. Stresses perpendicular to a face are defined as having two common indices; for example, a stress that is perpendicular to the face where the normal lies in the *x*-direction, is given by σ_{xx}. If the force is tangential, mixed subscripts are used. For example, σ_{xy} denotes a force acting in the *y*-direction along the face with normal in the *x*-direction. (b) In the continuum description, a stress σ_{xx} causes the object to extend in the *x*-direction, but also causes it to contract in the *y*- and *z*-directions. The ratio of the respective changes in length is the *Poisson* ratio

$$\boldsymbol{\sigma}_{xx} = E\boldsymbol{\epsilon}_{xx},$$

where $\boldsymbol{\sigma}_{xx}$ is the stress along the *x*-direction, ϵ_{xx} is the corresponding strain, and E is a proportionality constant known as *Young's modulus*. In contrast to the forces used to describe elastic behavior in one dimension, these surface forces (stresses) are expressed in the units of pressure (Newtons over area). Similarly, the deformation $\boldsymbol{\epsilon}$ is normalized so as to be unitless.

One thing that makes the continuous description different is that the stress in the *x* direction also leads to strains in both the *y* and *z* directions. For example, lengthening an object in the *x*-direction causes the cross-sectional area to contract (Figure 2b). Alternatively, we can see that stresses in the *y* and *z* directions also affect the strain in the *x*-direction. Thus, the strain in the *x*-direction can be expressed as

$$\epsilon_{xx} = \frac{1}{E}\left(\boldsymbol{\sigma}_{xx} - \nu\left(\boldsymbol{\sigma}_{yy} + \boldsymbol{\sigma}_{zz}\right)\right),$$

where the *Poisson ratio*, ν, quantifies the relative deformation in the planes away from which the stress is applied.

The strains described are normal as they result from stresses perpendicular to the face of the object. In contrast, those that act parallel to a face give rise to *shear* strains. In total, we describe the strains and stresses acting on the body by 3×3 tensors, $\boldsymbol{\epsilon}_{ij}$ and $\boldsymbol{\sigma}_{ij}$ where each index denotes one of the *x*, *y*, and *z* directions. In an elastic solid, the strain and stress tensors are proportional with the proportionality described by the constitutive equation $\boldsymbol{\sigma} = c\boldsymbol{\epsilon}$, where *c* is the *stiffness* tensor. In general, the stiffness tensor consists of 81 coefficients and can be written using four indices. In this case, the expression above can be written as

$$\boldsymbol{\sigma}_{ij} = \sum_{k}\sum_{\ell} c_{ijk\ell}\boldsymbol{\epsilon}_{k\ell},$$

where each index can be one of the three directions. In practice, because of symmetries and assuming an isotropic material this reduces to:

$$\boldsymbol{\sigma} = K(\mathrm{tr}\boldsymbol{\epsilon})I + 2G\left(\boldsymbol{\epsilon} - \frac{1}{3}(\mathrm{tr}\boldsymbol{\epsilon})I\right),$$

where the *bulk modulus*, *K*, describes the strain response of the object to a stress involving changes in volume but not shape, and the *shear modulus*, *G*, describes shape changes independent of volume changes. The two moduli are connected via the Poisson ratio ν:

$$K = \frac{2G}{3}\frac{1+\nu}{1-2\nu};$$

moreover, Young's modulus can be expressed in terms of either of these two moduli and the Poisson ratio:

$$E = 2G(1+\nu) = 3K(1-2\nu).$$

In the continuum description, viscoelasticity has a similar representation in which the stress tensor is replaced by the *stress rate tensor*:

$$\boldsymbol{\tau} = \boldsymbol{\mu}\,\dot{\boldsymbol{\epsilon}}\,,$$

where $\boldsymbol{\tau}$ is the *viscous stress tensor* and $\boldsymbol{\mu}$ is the *viscosity tensor*. Viscoelastic elements can display both possible behaviors. For example, a Kelvin–Voigt model would make the total stress the sum of the elastic and viscous stresses (Campbell & Bagchi, 2018):

$$\boldsymbol{\sigma} = \boldsymbol{\sigma}_{\text{elastic}} + \boldsymbol{\sigma}_{\text{viscous}} = c\boldsymbol{\epsilon} + \boldsymbol{\mu}\,\dot{\boldsymbol{\epsilon}}\,.$$

It is worth emphasizing that these are linear stress–strain relationships and are only accurate for small deformations. Larger deformations require nonlinear hyperelastic models such as the neo-Hookean solid (Arefi, Tsvirkun, Verdier, & Feng, 2020). A major drawback of these more realistic models, however, is the difficulty of parameterizing them based on experimental data (Fougeron et al., 2020; Mihai & Goriely, 2017; Valero, Navarro, Navajas, & García-Aznar, 2016).

2.3 | Potential energy

The mechanical properties of an object described above arise from the action of forces and torques on cell material (Mietke, Jülicher, & Sbalzarini, 2019). An alternative framework is to describe the system in terms of potential energy and to consider changes in shape as a minimization of energy functionals (Almendro-Vedia, Monroy, & Cao, 2013; Nakamura, Bessho, & Wada, 2013; Shlomovitz & Gov, 2008; Ujihara, Nakamura, Miyazaki, & Wada, 2010).

Mathematically, we define the potential energy as the integral of a force along a path. For example, a force F acting on an object that moves from point x_i to x_j requires work given by

$$\mathcal{W} = \int_{x_i}^{x_j} F(x')\cdot dx'.$$

The force is conservative if the energy does not depend on the path taken from x_i to x_j. As an example, consider the simple one-dimensional spring: $F = kx$ and take one point to be the resting length ($x_i = 0$) and the other point as the extension of the spring ($x_j = x$) the work required is

$$\mathcal{W}(x) = \int_0^x F(x')\cdot dx' = \frac{1}{2}k\|x\|^2.$$

The elastic potential energy stored in the spring is $-\mathcal{W}(x)$ under the principle that the work done by a conservative force and the change in potential energy sum to zero. This property can be turned around so that, given a potential energy function $\mathcal{W}(x)$, we can associate a force

$$F = -\frac{\partial \mathcal{W}(x)}{\partial x}. \tag{2}$$

This approach can be used even when the energy function is not a true energy in the sense of physics. The force defined above drives the system to its minimal energy state. For example, an "area expansion" energy (Ujihara et al., 2010) can describe the deviation of the area enclosed by a curve Γ from its resting area A_0 by

$$\mathcal{H}_{\text{area}}(x) = \frac{1}{2}k_{\text{area}}(A - A_0)^2, \quad A = \int_\Gamma dS,$$

where the integral denotes the current area. We can define an area restoring force as the functional derivative

$$F_{\text{area}}(x) = -\frac{\partial \mathcal{H}_{\text{area}}}{\partial A} = -k_{\text{area}}(A - A_0)n, \tag{3}$$

which drives the area towards A_0. The parameter k_{area} specifies the speed at which the system returns to its equilibrium area. Similar expressions are possible to ensure volume conservation (Shao, Rappel, & Levine, 2010).

In mechanical models of cells, a commonly used energy function is the *Helfrich energy functional* (Helfrich, 1973), which describes the elastic bending energy of a two-dimensional membrane of negligible thickness h surrounding a cell

$$\mathcal{H}_{\text{Helfrich}} = \int_\Gamma \left(K_0 + K(\kappa - \kappa_0)^2 + K_G\kappa_G\right) dS.$$

Here K_0 is the *surface tension* (described in more detail below), K and K_G are the *bending* and *saddle splay* moduli, respectively, κ and κ_G are the mean and Gaussian curvatures, respectively, κ_0 is the spontaneous curvature and the integral is taken over the whole surface area of the membrane. If the topology of the surface is unaltered, then the last component is constant (by the Gauss–Bonnet theorem) and can therefore be omitted from the minimization. Note the similarity between the second term and the area energy term described above. In fact, the change in area terms depend on terms κ and κ_0 are related to the change in area A is proportional to the product of the membrane thickness h and total mean curvature $\int_\Gamma \kappa\, dS$ so that the area energy and the second term of the Helfrich bending energy are proportional to each other. Based on the Helfrich energy, one can obtain equivalent forces by taking the functional derivative with respect to the positions. This, however, is far from trivial because the complex relationship between curvatures and positions (Guckenberger & Gekle, 2017).

2.4 | Surface tension

Cells have a cortical tension, which can be compared to the surface tension of a liquid. In this case, molecules at the surface of a liquid have higher potential energy than those in the bulk. The resultant *surface tension* can be considered as the energy cost for adding surface area to the cell. The liquid minimizes this energy by achieving minimum surface area, leading to a spherical shape at the interphase. The relationship between the resultant shape and pressure difference across the interphase is given by the Young–Laplace formula:

$$\Delta p = 2\gamma\kappa,$$

where K is, as above, the mean curvature of the surface (which for a sphere of radius R is $2/R$). The parameter γ is the surface tension and has units of force over length or energy over area. Though this equation is valid when the forces (pressures) are balanced, it can be used to drive cellular deformation by taking the stress proportional to a local mean curvature. Equivalently, the energy functional

$$\mathcal{H}_{\text{tension}} = \int_\Gamma \gamma\, dS$$

can be used to obtain a tension-force. Note that this constant term is the first term of the Helfrich energy.

3 | SIMULATION METHODS

Biochemical pathways regulate much of the cellular mechanics that acts to resist forces. For example, while localization of myosin to the rear of a migrating cell can lead to contractile stresses that can deform the cell, the high concentration

of myosin at the rear can also alter the cell's local viscoelastic properties through a process of strain stiffening, thus resisting further deformation (Brill-Karniely et al., 2014; Gardel et al., 2004; Kouwer et al., 2013; Reichl et al., 2008; Storm, Pastore, MacKintosh, Lubensky, & Janmey, 2005).

The intertwining between biochemistry and physics makes the study of cell shape changes an inherently complex one in which mathematical models are necessary. This is, by no means, trivial. Most biochemical models are based on reaction–diffusion equations that describe the temporal and spatial evolution of specific chemical species as they interact. Because of the large number of chemical species, it becomes quite computationally intensive to track their evolution over time. Few biological processes are able to be defined analytically, which requires numerical simulation techniques to be used instead. Simulating systems in which the cell shape is evolving lead to an even harder task. In mathematics, these are known as free-boundary problems, because the boundary between subdomains (e.g., the cell and its environment) changes over time. This evolution is governed by biochemical pathways (e.g., actin polymerization leading to pseudopod protrusive stresses) and/or purely mechanical (e.g., surface tension).

3.1 | Biochemical models

Simulations of complex biochemical signals are usually carried out using reaction–diffusion equations. Consider a set of regulatory species with concentrations denoted by c_i. This value changes according to

$$\frac{\partial c_i}{\partial t} = D\nabla^2 c_i + f_i(c), \tag{4}$$

where D is the diffusion coefficient, ∇^2 is the Laplace operator, and $f(c)$ is a (usually nonlinear) function of the concentrations of all the species that interact with c_i. This partial differential equation requires initial and boundary conditions.

Various simulations techniques can be used to simulate systems which have a fixed spatial geometry. During the last 20 years, a number of packages have appeared that aim to specialize these approaches to problems in cell signaling. For example, the Virtual Cell allows for spatial deterministic and stochastic simulations, as well the ability to generate geometries from two- and three-dimensional images, while providing a biology-based interface (Cowan, Moraru, Schaff, Slepchenko, & Loew, 2012; Resasco et al., 2012; Schaff, Gao, Li, Novak, & Slepchenko, 2016). Other spatial simulations include Smoldyn (Andrews, 2012), URDME (Drawert, Engblom, & Hellander, 2012), and Spatiocyte (Arjunan, Miyauchi, Iwamoto, & Takahashi, 2020). An important feature of most of these packages is the ability to describe the model in a freely exchangeable format. Recently, the systems biology markup language published their Level 3 specifications that allow for descriptions of spatial process (Ii et al., 2019; Keating et al., 2020).

What makes the problem we consider particularly challenging, however, is that the spatial domain over which these reaction–diffusion equations are solved is not fixed but changes as the geometry of the cell evolves. Moreover, these changes in morphology usually arise from actions regulated by these species. How to deal with these changes requires sophisticated numerical methods. Here we give an overview of some of the more popular approaches ones.

3.2 | Finite element methods

The finite element method (FEM) refers to a general approach used to solve partial differential equations on complex geometries. One of the original uses of FEM was to solve engineering problems of structural mechanics and fluid dynamics (Dhatt, Touzot, & Lefrançois, 2012; Zienkiewicz & Taylor, 2000). As such, it has been a common means of studying problems in biomechanics, such as bone remodeling (Mukherjee, Nazemi, Jonkers, & Geris, 2020; Müller & Rüegsegger, 1995) and, more recently, in cellular mechanics (Bidhendi & Geitmann, 2018; Ganesh, Laughrey, Niroobakhsh, & Lara-Castillo, 2020; Kennaway & Coen, 2019). In terms of simulating moving boundary problems, the FEM is an example of an interphase-tracking approach (Elgeti & Sauerland, 2016), whereby the positions of individual elements that form the deforming boundary are updated over time. This tracking represents a Lagrangian description.

A key first step in the process of the FEM is to subdivide the geometry into smaller regions—the eponymous finite elements—which is done through meshing (Figure 3a). This spatial discretization has a number of desirable features. It makes it easier to consider subdomains with varying properties. For example, different mechanical properties of the

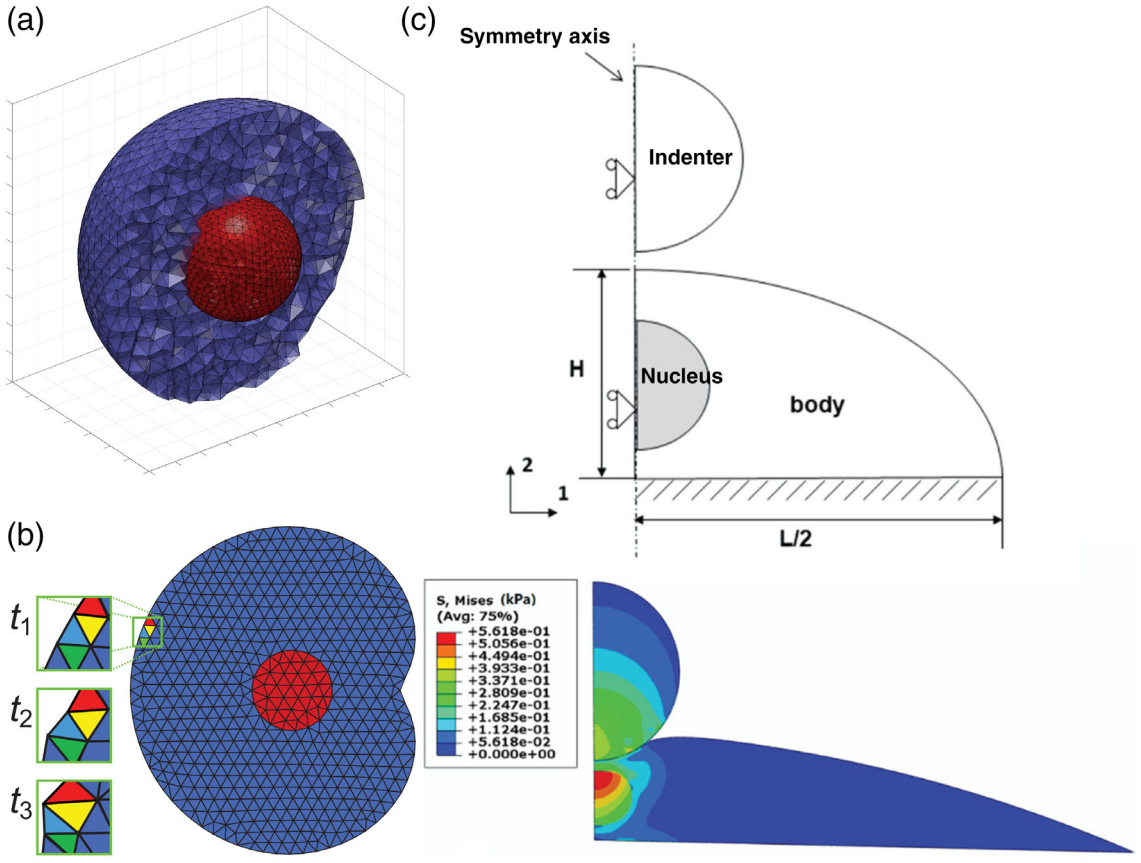

FIGURE 3 Finite element method. (a) Example of a meshing for two objects. The inner sphere represents a nucleus; the outer, which is only partially shown, is the cytoplasm. (b) Remeshing in a moving boundary. As the object deforms, the elements change shape. The three insets show how the elements change shape and size. How to account for these changes is a particularly challenging task in using FEM in moving boundary problems. (c) FE simulation result showing the stress on a cell that is being indented with a spherical indenter. The top plot shows the relative dimensions of the three objects included in the simulations: the cell body surrounding the nucleus and the spherical indenter. The bottom figure shows stress contour plots at an indentation depth of 1.5 μm (Reprinted with permission from Tang, Galluzzi, Zhang, Shen, and Stadler (2019). Copyright 2019 American Chemical Society)

nucleus, cytoplasm, and cortex (Bansod, Matsumoto, Nagayama, & Bursa, 2018; Katti & Katti, 2017) or incorporating extracellular structures like the extracellular matrix (ECM) (Kim, Silberberg, Abeyaratne, Kamm, & Asada, 2018) or hydrogels (Tang et al., 2019). It also turns the steady-state problems into algebraic ones and the transient problems into ordinary differential equations. The second step in the FEM is to rewrite the constitutive laws in terms of test functions that approximate the desired variables. The mathematics of this latter step is far from trivial, but there are many computational platforms that carry this out, discussed below.

The discretization process can be done using computer-aided design software and is usually based on simple geometrical elements. In fact, most initial models of cell migration start with circular/spherical shapes that are then evolved. Alternatively, segmented images of cell shapes can be used for the cell boundary which can then be meshed for the simulations (Schneider & Haugh, 2005). The meshing process involves choices both of the types and number of elements. In two-dimensions, the elements are typically triangles; in three-dimensions, tetrahedrons. Reducing the overall element size usually improves the accuracy of the simulations but at greater computational cost. Alternatively, the accuracy of the meshing can be improved by replacing these basic shapes by including nodes between the basic ones. For example, though a 2D triangle is defined by three points with a straight line joining each pair of points, it is possible to include an extra point in each edge thereby replacing the straight lines with second order lines (parabolas). This can have the effect of improving the meshing without having to include more elements. It is important to note that the mesh size need not be the same everywhere and that the mesh can be refined adaptively based on estimates of the local error.

While the initial meshing process is important, when modeling cell shape *changes*, remeshing will likely be required and so efficient means of doing so are needed (Figure 3b). How to update the mesh in an important consideration

because of the computational cost of doing so. Barrett, Garcke, and Nürnberg (2007) developed a means for moving the FE mesh according to curvature and other flows which they termed the *parameterized FEM*. This technique was adapted by Neilson, Mackenzie, Webb, and Insall (2010) to enable local velocity to depend on the concentration of various signaling molecules that are updated using reaction–diffusion equations. Elliott, Stinner, and Venkataraman (2012) have extended this work into three dimensions and included bending energy.

The mechanical models described above can be easily used in the FEM. For example, Teo, Goryachev, Parker, and Chiam (2010) studied the deformation of single, suspended fibroblasts in an optical stretcher. They assumed a heterogeneous mechanical model in which the cell was divided into a mostly elastic cortical region and a viscous cytoplasm, similar to that of Figure 1d. However, within each of the compartments, the viscoelastic parameters were also allowed to vary radially.

More complex mechanics can also be considered. For example, Zhou, Xu, Quek, and Lim (2012) used FEM to simulate micropipette aspiration on fibroblasts under various mechanical loadings using a mechanical model that aims to recreate a power-law rheology model. Bansod et al. (2018) recreated micropipette aspiration and atomic force microscopy (AFM) experiments using a hybrid approach that combined a neo-Hookean solid with shear modulus and linear elastic cytoskeletal elements representing actin and microtubule filaments. AFM indentation was also simulated and compared to a FEM with the goal of understanding the effect of geometrical and mechanical properties of constitutive parts such as the cell body, nucleus, and lamellipodium (Tang et al., 2019); see Figure 3c.

3.2.1 | Software available

Because of its long history and broad range of applications, there are numerous computational packages for using the FEM to solve partial differential equations. Commercial versions include Ansys (Canonsburg, PA), Abaqus FEA (Dassault Systèmes, Johnston, RI), and Comsol Multiphysics (Burlington, MA) which are general purpose finite element analysis software suites. A general purpose open-source package is FEniCS (Langtangen, 2012). FEBio is another-source software suite that was specifically developed with the purpose of solving problems in computational solid biomechanics (Maas, Ellis, Ateshian, & Weiss, 2012). Recent upgrades allow for the consideration of shell elements in cell mechanics analyses (Hou, Maas, Weiss, & Ateshian, 2018) and the ability to extend the program through plugins (Maas, LaBelle, Ateshian, & Weiss, 2018).

3.3 | Immersed boundary method

The immersed boundary method (IBM) was developed by Peskin (1972) in his doctoral thesis as a means of simulating the interaction between fluids and biological structures (Peskin, 2002). Though originally developed as a means of studying fluid dynamics of blood flow around the heart, it has been used to describe the motion of individual cells. The technique involves two types of variables (Figure 4a). The equation of motion of the fluid can be described by the Navier–Stokes equation

$$\rho\left(\frac{\partial v}{\partial t}+v\cdot\nabla v\right)=-\nabla p+\mu\nabla^2 v+F,$$

where $v(x, t)$ denotes the local fluid velocity, $p(x, t)$ the pressure, ρ the fluid density, μ the dynamic viscosity, and $F(x, t)$ includes all the external forces acting on the fluid. For incompressible fluid we have that $\nabla\cdot v = 0$. In the case of single cell organisms in which inertial forces are negligible compared to the viscous forces (i.e., the Reynolds number is much smaller than one), the simpler Stokes equation is used and is obtained by setting the left-hand side equal to zero. In the IBM, the fluid velocity is computed using a fixed, *Eulerian*, grid.

In contrast, Lagrangian variables are defined on a moving mesh representing the cell boundary. These can be joined by elastic links obeying Hooke's law and having a set resting length. These nodes surround a viscous incompressible fluid (Vanderlei, Feng, & Edelstein-Keshet, 2011) or a secondary set of nodes representative of the actin cytoskeleton (Bottino, 1998; Bottino, Mogilner, Roberts, Stewart, & Oster, 2002). At every time point in the simulation, the position of each boundary point is used to calculate elastic stresses on each node. Forces acting on each boundary point may also arise from active forces such as actin polymerization or actomyosin contraction.

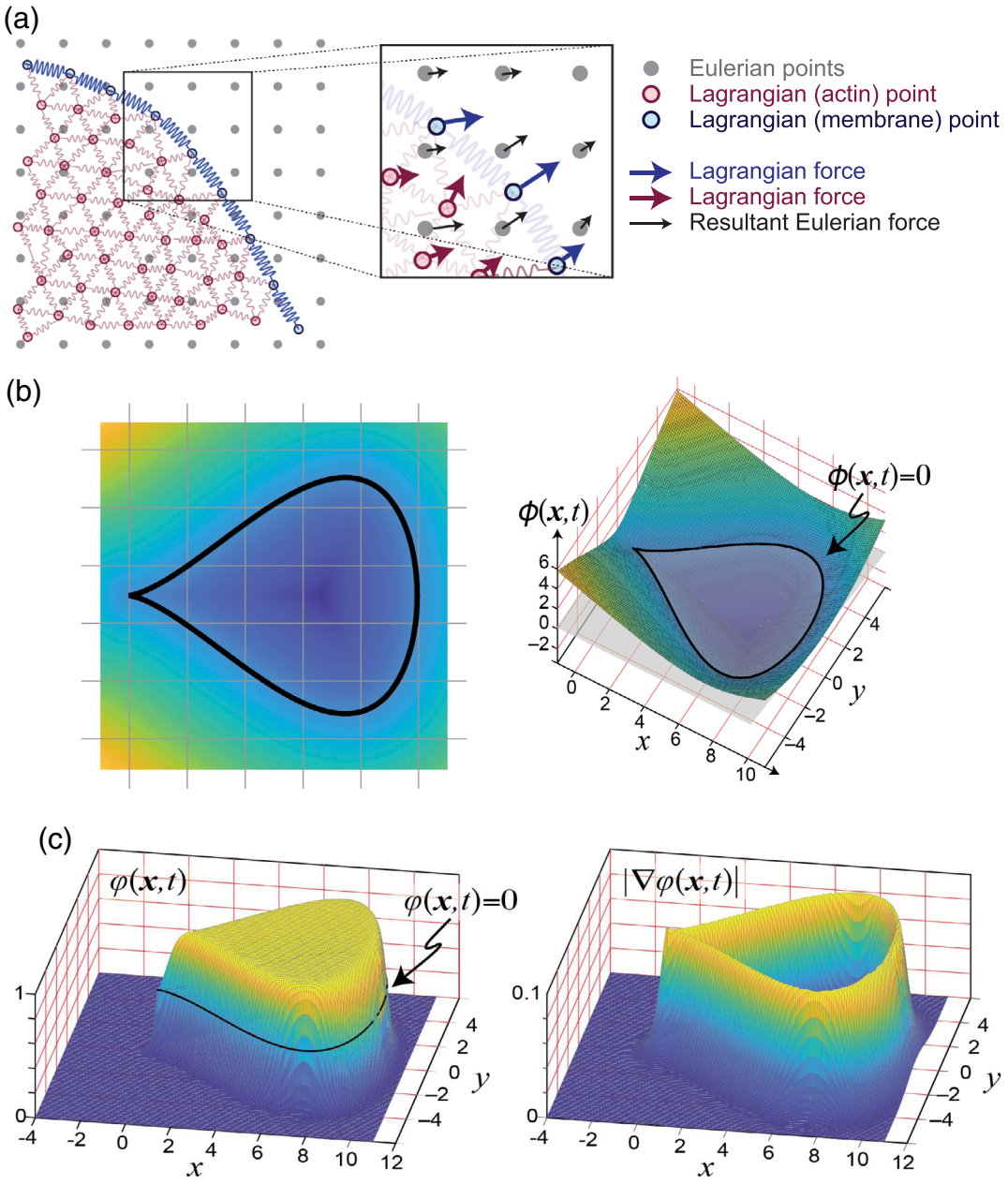

FIGURE 4 Immersed boundary, level set and phase field methods. (a) This shows the two sets of nodes needed in the IBM. The Eulerian points are defined on a fixed grid and are used to track the fluid. The Lagrangian mesh is used to specify the cell's evolution. It can consist of membrane points alone, or membrane/cytosol points. The forces on the Lagrangian network are spread to the fluid based on their location. The fluid velocity is used to upgrade the location of the Lagrangian nodes. (b) Signed distance function used to define shape in the LSM. Along the Cartesian grid, the distance of every point to the initial shape (in black) is calculated with a positive or negative sign for points outside or inside, respectively, of the region. This forms the level set function $\phi(x, t)$ which is updated over time. (c) Example of a PFM φ (x, t) (left) and magnitude of the gradient $\|\nabla\varphi(x, t)\|$. The cells in panels b and c have the same shape

The net sum of the forces acting on the Lagrangian nodes is used to update the local fluid velocity. As shown in Figure 4a, the membrane nodes need not coincide with the nodes used to update the fluid, so these forces are spread among the nearest points on the fluid grid and are used to update the fluid velocity. Once the fluid velocity field is updated the boundary points are then moved at the local fluid velocity. Note that the IBM requires the solution of the two set of variables, and these equations are often solved using FEM, particularly for the Lagrangian variables (Guckenberger & Gekle, 2017).

As described above, the IBM explains how the forces from one set of variables affects the motion of the other. However, it does not describe the temporal and spatial variations in the intracellular species that gives rise to many of these forces. In a static computational environment, this is achieved by solving partial differential equations association with reaction–diffusion processes having the form of Equation (4). If the domain representing the cell is immersed in a fluid with velocity v, then the species will be carried along by the fluid. In this case the advection term $v \cdot \nabla c$ must be added to the left-hand side; that is

$$\frac{\partial c_i}{\partial t} + v \cdot \nabla c_i = D\nabla^2 c_i + f_i(c)$$

now describes the concentration of the species. We must also consider the boundary term. Assuming that the species must stay inside the cell, we have that

$$n \cdot \nabla c = 0$$

around the boundary with normal n. Several methods have been used for solving these equations. One is to solve this at the fixed grid points used to solve for the fluid, where the velocity field is available (Dillon & Othmer, 1999). In this case care must be taken near the boundary to determine which points lie inside the closed cell. An alternative method is to solve the equations on an irregular grid defined by the internal nodes (e.g., the actin nodes of Figure 4a). In this case, the advection term is not needed because the Lagrangian is a moving frame of reference (Bottino, 2001).

The interior of the cell is partitioned according to a *Voronoi tessellation*, that is, for each node A_i the set Ω_i denotes all points that are closest to node i than any other node. If N_i denotes the set of neighboring nodes to A_i (the nodes A_j for which Ω_i and Ω_j share an edge) then it is possible to approximate the diffusion of c as

$$\nabla^2 c_i = \frac{1}{\Omega_i} \sum_{j \in N_i} \frac{c_j - c_i}{\|A_j - A_i\|} |s_{ij}|,$$

where c_i and A_i are the concentration and area at node i and s_{ij} is the distance between the two nodes (Bottino, 2001). One drawback of this scheme, however, is that the Voronoi tessellation and associated Delaunay triangulation must be updated at each time step and this can be computationally expensive.

While it is fair to say that the IBM is more commonly used in simulations involving blood flow and the heart which do not satisfy the Stokes equation assumption, nevertheless, the IBM has been employed recently to model cell growth and contractile ring-driven cytokinesis in three dimensions (Bächer & Gekle, 2019; Lee, 2018; Li & Kim, 2016). These models do not consider reactions or signaling components; rather, the contractile ring is imposed as a force which drives constriction.

For examples of signaling components driving cell migration, Campbell and Bagchi (2017, 2018) coupled the IBM to an activator-inhibitor model of reaction dynamics to simulate cell motion in three-dimensions with and without obstacles. The reaction–diffusion equations that governed these terms were solved using FEM as in Elliott et al. (2012).

3.3.1 | Software available

Over the years, numerous implementations for the IBM have been developed. Among the open source packages is IBAMR (Griffith, 2020) which offers parallel implementation and adaptive mesh refinement. Recently, Battista, Strickland, and Miller (2017) published IB2d, an IBM implementation in both Matlab and python that supports two-dimensional simulations, as well as advection–diffusion of chemical gradients.

3.4 | Level set methods

Level set methods (LSMs) denote a set of numerical techniques developed to track the evolution of interphases. Originally developed by Osher and Sethian (1988) to simulate propagating front with curvature-dependent speeds, it has

gained a great following, particularly in the fields of image processing and computer graphics (Osher & Fedkiw, 2003; Sethian, 1999). It has been used to study cell migration (Gallinato, Ohta, Poignard, & Suzuki, 2017; Miao et al., 2017, 2019; Neilson et al., 2011; Shi, Huang, Devreotes, & Iglesias, 2013; Wolgemuth & Zajac, 2010; Yang et al., 2008), cell division (Poirier, Ng, Robinson, & Iglesias, 2012), wound healing (Ben Amar & Wu, 2014), cell and tissue growth (Alias & Buenzli, 2020; Guyot et al., 2014; Guyot, Papantoniou, Luyten, & Geris, 2016; Guyot, Luyten, Schrooten, Papantoniou, & Geris, 2015), and mechanosensation (Zhang, Rosakis, Hou, & Ravichandran, 2020).

LSMs are based on an implicit scheme for defining arbitrary surfaces. The boundary of an object, denoted by $\Gamma(t)$, is defined as the zero-level contour of a potential function, $\phi(x)$, that is defined in one dimension higher than the shape that is to be tracked. For example, the two-dimensional shape seen in Figure 4b is the set of all points (x, y) that satisfy $\phi(x, y) = 0$. Over time, the boundary of this region obeys the evolution equation

$$\frac{\partial \phi}{\partial t} + \nabla \phi \cdot v = 0, \tag{5}$$

where $v(x)$ is the interphase velocity. For a shape defined as the level set of a function ϕ, the normal direction of the surface is given by

$$n = \frac{\nabla \phi}{\|\nabla \phi\|}.$$

It follows from Equation (5) that only the normal component of the velocity that influences the evolution equation. Moreover, if the velocity is normal to the surface, $v = Fn$, the level-set equation can be written as

$$\frac{\partial \phi}{\partial t} + F\|\nabla \phi\| = 0.$$

An advantage of the LSM is that the evolution of the shape is achieved by updating ϕ which is defined on a fixed Cartesian grid and thus eliminates the need to parameterize the boundary or to update the grid. A disadvantage, however, is that the function ϕ is defined in one dimension higher than that of the cell, and hence can lead to more expensive computations. Solutions to the latter have included the narrow-band method in which the solution of ϕ is updated only in a narrow neighborhood of the interphase (Adalsteinsson & Sethian, 1995).

Though it is possible to choose different potential functions to denote the interphase, there are particular numerical advantages in choosing $\phi(x, t)$ to be a *signed distance function*, defined as the distance from the point x to the boundary $\Gamma(t)$:

$$\phi(x,t) = \pm \min_{x^* \in \Gamma(t)} \left\| x - x^* \right\|$$

where the sign is chosen so that it is $+1$ for points outside the region and -1 inside (Figure 4b). For example, for a signed distance function, the normal equation above reduces to $n = \nabla \phi$. Over time, as the level set function ϕ evolves, it may deviate from the signed distance function because of computational errors. This will require the reinitialization equation:

$$\frac{\partial \phi}{\partial t} + \text{sign}(\phi)(\|\nabla \phi\| - 1) = 0.$$

3.4.1 | Implementing forces in the LSM

The evolution of the surface in the LSM is governed by the level-set Equation (5). Updating ϕ requires the velocity of the membrane normal to the surface. To this end, we can compute the velocity by considering the strain according to the mechanical models described in Section 2. For example, using the viscoelastic model of Figure 1d, the total strain

normal to the surface obeys the second-order differential equation Equation (1) where $\boldsymbol{\sigma}$ represents the total stress normal to the surface at each point along the interphase. This stress will have passive components, such as those arising from surface tension or area/volume conservation, active components such as actin-driven protrusion or actomyosin contractility, or externally applied including those from a micropipette aspirator, an AFM probe, and so on. Because the model is linear, we can consider each stress individually. For example,

$$\boldsymbol{\sigma} = \boldsymbol{\sigma}_{\text{ten}} + \boldsymbol{\sigma}_{\text{vol}} + \boldsymbol{\sigma}_{\text{pro}} + \boldsymbol{\sigma}_{\text{ret}} + \boldsymbol{\sigma}_{\text{ext}},$$

where the terms on the right-hand side represent contributions of surface tension, volume conservation, protrusive, and retraction forces, and any imposed external forces, respectively. For example, following the Young–Laplace equation, surface tension stress is proportional to the local curvature at the surface:

$$\boldsymbol{\sigma}_{\text{ten}} = \gamma_{\text{ten}} \kappa(x,t).$$

As the boundary is defined implicitly by the implicit level set function, the mean curvature $\kappa(x)$ is the divergence of the unit normal vector:

$$\kappa = \nabla \cdot n.$$

If ϕ is a signed-distance function, this simplifies greatly

$$\boldsymbol{\sigma}_{\text{ten}} = \gamma_{\text{ten}} \nabla^2 \phi.$$

Note that the last term is now a linear function of ϕ.

Other forces are straightforward to implement. For example, an area/volume conservation stress can be implemented as in Equation (3).

$$\boldsymbol{\sigma}_{\text{vol}} = \gamma_{\text{vol}} (V - V_0) n.$$

The net stresses lead to a membrane deformation strain according to Equation (1). This velocity vector v is defined for all points on the cell membrane and acts normal to the boundary. To solve the level-set equation, however, requires that a velocity be available at all points. A velocity field that minimizes the normal component of the field variation is achieved by setting the velocity at points x away from the membrane equal to the membrane velocity at the location on the boundary (Γ) closest to the point x. Zhao, Chan, Merriman, and Osher (1996) show that a signed distance function tends to keep this property when the closest neighbor extrapolation method is used.

3.4.2 | Implementing reaction–diffusion equations

One of the difficulties of using the LSM for simulating coupled mechano-chemical systems is that the LSM concerns itself only with the interphase of two structures. As the surface evolves, there is no inherent coupling of points over time. Several methods have been proposed for overcoming this.

Adalsteinsson and Sethian (2003) included variables that exist only on the boundary, say f_B, and approximating them by a globally defined f that agrees on the front. They developed formulae describing how diffusion and advection evolved as the boundary, defined implicitly by the level-set function ϕ, changed. To this end they incorporated a second equation

$$\frac{\partial f}{\partial t} + v \cdot \nabla f = 0,$$

where the function f denotes the approximation of the interfacial data and v is the velocity of the function ϕ. Alternatively, Pons, Hermosillo, Keriven, and Faugeras (2006) developed a computational technique for establishing a correspondence between points on the surface at two time points during the evolution. More recent improvements on this method are found in Bellotti and Theillard (2019).

A finite volume method has also been used to couple the LSM to associated reaction–diffusion equations (Strychalski, Adalsteinsson, & Elston, 2010; Wolgemuth & Zajac, 2010). This uses the distance function ϕ to construct a resolved finite volume discretization of the geometry. The contents of each finite volume are then evolved between two different time steps ensuring that overall mass is conserved.

3.4.3 | Software available

The numerical solution of the level-set equation is by-no-means trivial; see Osher and Fedkiw (2003) for a discussion of such algorithms. In theory, because the LSM is based on partial differential equations, any software package that can solve these equations can be used to model cell shape change using this method. An excellent Matlab toolbox for solving level-set equations was developed by Mitchell (2008), and is freely available.

3.5 | Phase field methods

The phase field method (PFM) is an alternative method for describing interphasial dynamics. Originally developed to solve physical problems of phase separation that have well defined energy functionals (Cahn & Hilliard, 1958), it has been adapted to simulate systems with moving boundaries. In particular, numerous applications have appeared which rely of PFM for simulating cell migration (Alonso, Stange, & Beta, 2018; Bresler, Palmieri, & Grant, 2019; Camley et al., 2014; Cao et al., 2019; Gomez, Bures, & Moure, 2019; Kulawiak, Camley, & Rappel, 2016; Löber, Ziebert, & Aranson, 2015; Molina & Yamamoto, 2019; Moure & Gomez, 2018; Moure & Gomez, 2020a, 2020b; Shao et al., 2010; Shao, Levine, & Rappel, 2012; Tao et al., 2020) and, to a lesser degree, cytokinesis (Zhao & Wang, 2016a, 2016b).

The phase field approach shares some similarities with the LSM including the fact that the interphase is defined implicitly by an auxiliary field function, φ, defined everywhere. This function assumes distinct values in the two phases (for example, one inside the cell and zero outside) and interpolates continuously across a thin interphase. To see how the interphase arises, consider the function

$$h(\varphi) = \frac{1}{4}\varphi^2(1-\varphi)^2,$$

which represents a double-well potential with minima at zero and one. The associated differential equation

$$\frac{\partial \varphi(x,t)}{\partial t} = -\frac{\alpha}{\epsilon}h'(\varphi) = -\frac{\alpha}{\epsilon}\varphi(1-\varphi)\left(\frac{1}{2}-\varphi\right) \tag{6}$$

has two homogeneous, stable, steady-state solutions at the minima, and one unstable solution at $\varphi(x) = 1/2$. The addition of a diffusion-like term

$$\frac{\partial \varphi}{\partial t} = \epsilon\nabla^2\varphi - \frac{\alpha}{\epsilon}h'(\varphi) \tag{7}$$

leads to a partial differential equation. Assuming that the space is one-dimensional, and has boundary conditions at the two stable equilibria, $\varphi(-\infty) = 0$ and $\varphi(\infty) = 1$, the steady-state solution $\bar{\varphi}(x)$ represents a smooth transition between the two stable values. In one dimension, $\bar{\varphi}(x)$ has the hyperbolic tangent shape

$$\bar{\varphi}(x) = \frac{1}{2} + \frac{1}{2}\tanh(c(x-x_0)), \quad c = \frac{1}{\epsilon}\sqrt{\alpha},$$

where the transition is centered at x_0 and the parameter ϵ controls the width of the interphase; smaller values of ϵ lead to sharper interphases. Note that, if $d(x)$ is the signed distance function of the LSM, then the function $\bar{\varphi}(x)$ in the PFM is given by $\varphi(x) = \tanh\left(d(x)/\sqrt{2\epsilon}\right)$ (Gomez et al., 2019). In modeling cells, the initial conditions can be set so that φ is one inside the cell and zero outside (Figure 4c).

While the location of the interphase is stationary, it can be made to move in either direction. One way of doing this is to replace the unstable equilibrium $\varphi = 1/2$ with a number λ between zero and one. If $\lambda > 1/2$ then the interphase moves towards the left; alternatively, if $\lambda < 1/2$, then the interphase moves to the right. Thus, one way of moving the boundary is to replace the right-hand term in Equation (7) with a term:

$$\frac{\partial \varphi(x,t)}{\partial t} = \epsilon \nabla^2 \varphi - \frac{\alpha}{\epsilon}\varphi(1-\varphi)\left(\frac{1}{2} + u - \varphi\right). \tag{8}$$

Changing the sign of u determines the direction of movement. For example, one possible way of varying u is to use it to couple it to volume/area conservation (Ziebert & Aranson, 2013). For example, let

$$u(\varphi) = \int_\Gamma \varphi \, dV - V_0, \tag{9}$$

where V_0 is the resting area/volume of the cell. Note that if φ were perfectly one inside the cell and zero outside, then the integral equals the volume of the cell. If this is bigger than V_0, then $u(\varphi) > 0$ and the interphase moves so as to shrink the cell towards its resting volume. Ziebert and Aranson (2013) have also coupled the phase-field equation to a *polarization* vector p that drives protrusion directionally. This can be thought of as being proportional to actin polymerization. The vector p can be made to act on the membrane by multiplying by the gradient of the function φ. It then affects the field by changing Equations (8) and (9) to

$$\frac{\partial \varphi(x,t)}{\partial t} = \epsilon \nabla^2 \varphi - \frac{\alpha}{\epsilon}\varphi(1-\varphi)\left(\frac{1}{2} + u - \varphi\right) - \beta p \cdot (\nabla \varphi)$$

and

$$u(\varphi) = \left(\int_\Gamma \varphi \, dV - V_0\right) - \sigma \|p\|^2,$$

respectively. Here, σ is a parameter that regulates cell shape (Löber et al., 2015; Molina & Yamamoto, 2019; Ziebert & Aranson, 2013).

3.5.1 | Implementing forces in the PFM

An alternative way of directing cell motion is to consider forces and their associated energy functionals. In fact, the evolution of φ is determined by the dissipative minimization of a free energy functional. The right-hand side of the phase-field Equation (6) has a well-defined interpretation in terms of energy. Specifically, a free energy can be defined which depends on φ and the gradient $\nabla\varphi$ (Cahn & Hilliard, 1958):

$$\Psi(\varphi) = \gamma\left(\frac{\epsilon}{2}\|\nabla\varphi\|^2 + \frac{\alpha}{\epsilon}h(\varphi)\right),$$

leading to the Ginzburg–Landau free energy functional

$$\mathcal{H} = \int_\Omega \Psi \, dx = \gamma \int \left(\frac{\epsilon}{2}\|\nabla\varphi\|^2 + \frac{\alpha}{\epsilon}h(\varphi)\right) dx.$$

The corresponding force density follows from the virtual work principle described in Equation (2)

$$F_{\text{ten}} = -\frac{\delta \mathcal{H}(x)}{\delta x} = \frac{\partial \mathcal{H}(x)}{\partial \phi}\nabla\varphi = -\gamma\left(\epsilon\nabla^2\varphi - \frac{\alpha}{\epsilon}h'\right)\nabla\varphi.$$

The term in the brackets is just the right-hand side of Equation (7). In fact, this shows that the phase-field equation is the gradient flow equation and this evolves to minimize the energy functional $\mathcal{H}$.

This approach can be extended to consider other energy functionals. For example, finding the function φ that minimizes the *elastic energy*

$$\mathcal{H} = \int_{\Omega} \frac{k\epsilon}{2} \left| \nabla^2 \varphi - \frac{1}{\epsilon^2} h(\varphi) \right|^2 dx$$

is equivalent to minimizing the bending energy in Helfrich's formulation with prescribed surface area and bulk volume constraints (Du, Liu, & Wang, 2004).

Two ways have been suggested for including these forces into the phase field equation. The first, introduced in Biben and Misbah (2003) and Biben, Kassner, and Misbah (2005) starts with the fact that the phase-field interphase is defined implicitly and hence satisfies the LSM Equation (5). It then appends terms proportional to F_{ten} and to curvature:

$$\frac{\partial \varphi}{\partial t} + v \cdot \nabla \varphi = k_1 F_{\text{ten}} + k_2 \kappa \|\nabla \varphi\|.$$

In this approach, the velocity follows from the Navier–Stokes equation, but assuming small Reynolds number:

$$\rho \frac{\partial v}{\partial t} \approx -\nabla p + \mu \nabla^2 v + F,$$

where external forces (e.g., protrusion, contraction, etc.) are added. This approach has been used extensively by Gomez and coworkers (Gomez et al., 2019; Moure & Gomez, 2018; Moure & Gomez, 2020a, 2020b).

An alternative approach, based on the work of Du et al. (2004) and used by Rappel and others (Alonso et al., 2018; Camley et al., 2014; Cao et al., 2019; Kulawiak et al., 2016; Shao et al., 2010, 2012; Tao et al., 2020), starts with the assumption that, in the low inertia limit, the sum of all forces is zero. Now, one of these forces is assumed to be frictional and to be proportional to cell velocity ($F_{\text{friction}} = -\tau v$) and hence

$$v = \frac{1}{\tau} \sum_{\text{other}} F.$$

The right-hand side can include the forces arising from the Helfrich bending and the tension force defined above. Note that the frictional assumption is equivalent to including a viscous term in the mechanical model. Other forces can be added. Shao et al. (2010), for example, include protrusive and retraction active forces

$$F_{\text{prot}} = -k_{\text{prot}} \frac{\nabla \varphi}{\|\nabla \varphi\|}, \quad F_{\text{ret}} = k_{\text{ret}} \frac{\nabla \varphi}{\|\nabla \varphi\|},$$

where the coefficients k_{prot} and k_{ret} are proportional to the local actin filaments and myosin motors, respectively. This v can be added to the PFM evolution equation leading to

$$\tau \frac{\partial \varphi}{\partial t} + \sum_{\text{other}} F \cdot \nabla \varphi = 0$$

or, for example, if the forces modeled are due to bending, protrusion, retraction, and area conservation, we get:

$$\tau \frac{\partial \varphi}{\partial t} = -\gamma \left(\epsilon \nabla^2 \varphi - \frac{\alpha}{\epsilon} h' \right) \nabla \varphi + k_{\text{prot}} \|\nabla \varphi\| - k_{\text{ret}} \|\nabla \varphi\| - k_{\text{area}} (A - A_0).$$

3.5.2 | Incorporating chemical species in the PFM

Incorporating chemical, reaction–diffusion equations in the PFM is relatively straightforward, as there are already indicator functions for both the interior of the cell (φ) and the membrane ($\delta_\varphi = \|\nabla\varphi\|$). For example, if a species with concentration c is found in the cytoplasm, then the product φc is restricted to the interior of the cell. Alternatively, the product $\delta_\varphi c$ restricts it to the narrow region around the interphase. Thus, the evolution of a species that is found in the cytoplasm is governed by

$$\frac{\partial(\varphi c_{\text{cyt}})}{\partial t} = \nabla\cdot\left(D_{\text{cyt}}\varphi\nabla c_{\text{cyt}}\right) + f_{\text{cyt}},$$

where f_{cyt} includes all the relevant reactions (Moure & Gomez, 2019). For a function found only on the membrane, the term φ in this equation would be replaced by δ_φ.

3.6 | Other modeling approaches

We have described the most common packages for coupling mechanics and reaction–diffusion equations. Nevertheless, there are a number of other modeling approaches that are also popular.

There are a number of papers that rely on *agent-based models* (ABMs). These models describe individual *agents* (e.g., microtubules, actin filaments, myosin motors, etc.) and simulate their interactions (Mogilner & Manhart, 2016). The models are typically coarse-grained so that they emphasize their interactions while eschewing the microscopic details. The diffusion of individual elements as well as their binding interactions is simulated via Langevin dynamics. For example, motor binding is simulated by first defining a region of capture for a filament/motor pair and then using a Monte Carlo step to determine whether the motor is captured. For example, Bidone et al. (2017) developed a three-dimensional model to account for various observed properties of the actomyosin network, including the role of actin crosslinking proteins in buckling. Using a similar agent-based two-dimensional model of the actomyosin network, Chanet et al. (2017) showed that the actomyosin network orients in response to mechanical constraints imposed by tissue shape. While most ABMs rely on custom-built software, Cytosim is an open-source package for simulating the cytoskeleton that has had an excellent record (Cortes, Gordon, Nédélec, & Maddox, 2020; Hannabuss et al., 2019).

Another alternative approach is the *cellular Potts methodology* (CPM). In the CPM, the cell is defined in a Euclidean lattice, where each of the elements is either in the cell or not. The evolution of these elements is governed by an energy functional, which can include components related to adhesion, growth, migration, so on. Forces and other mechanical properties of cells can be incorporated into the CPM via the energy terms (Rens & Edelstein-Keshet, 2019). The state of each element evolves using a Monte Carlo scheme by which energy is minimized over time. Software platforms for CPM include CompuCell3D (Swat et al., 2012) and Chaste (Mirams et al., 2013).

4 | BIOLOGICAL PROCESSES

The goal of mathematical models of cell physiology is to elucidate mechanisms and to test hypotheses that are difficult to test experimentally. It follows that a true test of the models is to determine what has been learned from these. Below we consider some of the biological processes that have used these methods.

4.1 | Cell migration: single cells

Motile cells come in various shapes. It is not surprising that one of the most active research areas for coupling chemical and mechanical signaling come in studies of cell motility. Mathematical models have had a significant impact; see Iglesias and Devreotes (2008), Roca-Cusachs, Sunyer, and Trepat (2013), Devreotes et al. (2017), and Rappel and Edelstein-Keshet (2017) for some relevant reviews.

4.1.1 | Keratocyte locomotion

The fan-like shape of keratocytes offers a relatively simple means for studying how shape arises from the cell's mechanical properties. Not surprisingly, it was one of the first cells to attract models of cell shape change. Rubinstein, Fournier, Jacobson, Verkhovsky, and Mogilner (2009) developed an early model of viscoelastic actin mechanics and myosin transport. They showed that myosin concentrated at the rear boundary and pulled the actin network inward so the centripetal actin flow is slow at the front, and faster at the rear and at the sides. Shao et al. (2012) recreated these results using the PFM and showed how different adhesion properties and myosin concentrations altered both the velocity and steady-state shape.

More recently, Nickaeen et al. (2017) considered lamellipodial motility and analyzed its dependence on three parameters: myosin-dependent contractility, a characteristic viscosity-adhesion length, and the rate of actin protrusions. They showed that, provided contractility was sufficiently high, cells could break symmetry leading to turning behavior.

4.1.2 | Amoeboid locomotion and the excitable system hypothesis

The motion of amoeboid cells, whether in random motility or in response to external chemoattractant signals is one of the areas that has received the most interest from modeling.

About a decade ago, the excitable system hypothesis posited that the random migration of cells such as neutrophils and amoebae was regulated by an excitable system (Hecht, Kessler, & Levine, 2010; Xiong et al., 2010). In this hypothesis, noise-driven firings of this system would give rise to actin polymerization that would drive pseudopods. Moreover, chemoattractants directed cell movement by biasing the probability that pseudopods would appear in one side of the cell. Several groups coupled these models to drive cell migration, first in two-dimensions (Hecht et al., 2011; Neilson et al., 2011; Shi et al., 2013) and, more recently in three-dimensions (Campbell & Bagchi, 2017, 2018; Cao et al., 2019). These models supported the hypothesis. In the absence of a chemoattract, the in silico cell created pseudopods that strongly resembled those seen experimentally. For example, a characteristic of pseudopods in *Dictyostelium* cells is that they appear to split (Bosgraaf & Van Haastert, 2009). Models that coupled excitability with the protrusive forces also displayed these splits (Figure 5a,b).

These models also coupled the external chemoattractant to directional motility. Models based on the local-excitation, global-inhibition (LEGI) premise (Levchenko & Iglesias, 2002; Parent & Devreotes, 1999) and those based on the model of Meinhardt (1999) showed similar response to chemoattractants. Moreover, these models showed the role of a memory or *polarization* in enabling persistent migration in the absence of chemoattractants. Interestingly, while the 2D models have now been expanded into three-dimensions, these more sophisticated models have mostly confirmed the results of the simpler 2D models. An interesting hypothesis, arising from these models is that chemotactic cells generate their own chemotactic gradients by locally consuming the chemoattractant (Mackenzie, Nolan, Rowlatt, & Insall, 2019).

Over the years, several models have suggested that cell morphology could be used to transition from one shape to another. For example, Satulovsky, Lui, and Wang (2008) altered various parameters, including strengths of adhesion, protrusion, and retraction and showed that different cell shapes could arise. Similarly, Nishimura, Ueda, and Sasai (2009) posited that localized cortical factors that suppress actin polymerization are diluted at the front and accumulate at the retracting rear of cell, thus establishing cell polarity. As the strength of these feedbacks grows or falls, the cell migration pattern changes. More recently, Niculescu, Textor, and de Boer (2015) used an actin-based feedback term into a CPM model of cell motility and showed that varying the strength of this feedback could lead to both keratocyte and amoeboid shapes. Through mathematical models, Zmurchok and Holmes (2020) have suggested that Rho GTPases regulate these shape changes.

Miao et al. (2017) used chemically induced dimerization to show that amoeboid cells could, in fact, be made to change migratory modes. The activity of the cell could be altered by altering the levels of various regulators in *Dictyostelium* cells leading to hyperactive cells in which actin-driven cellular protrusions expanded. These cells transitioned into keratocyte-like and oscillatory morphologies, as predicted from simulations. It was hypothesized that these changes in activity arose from a lowering of the threshold for activation of the excitable system. This was tested using the coupled excitable-system-mechanical models (Miao et al., 2017, 2019). In these models, the cells did acquire the oscillatory shape. Moreover, the models showed that it was only with a polarity/memory mechanism that the cell became fan-like. Using a three-dimensional PFM model, Cao et al. (2019) reproduced these migration modes generated and also

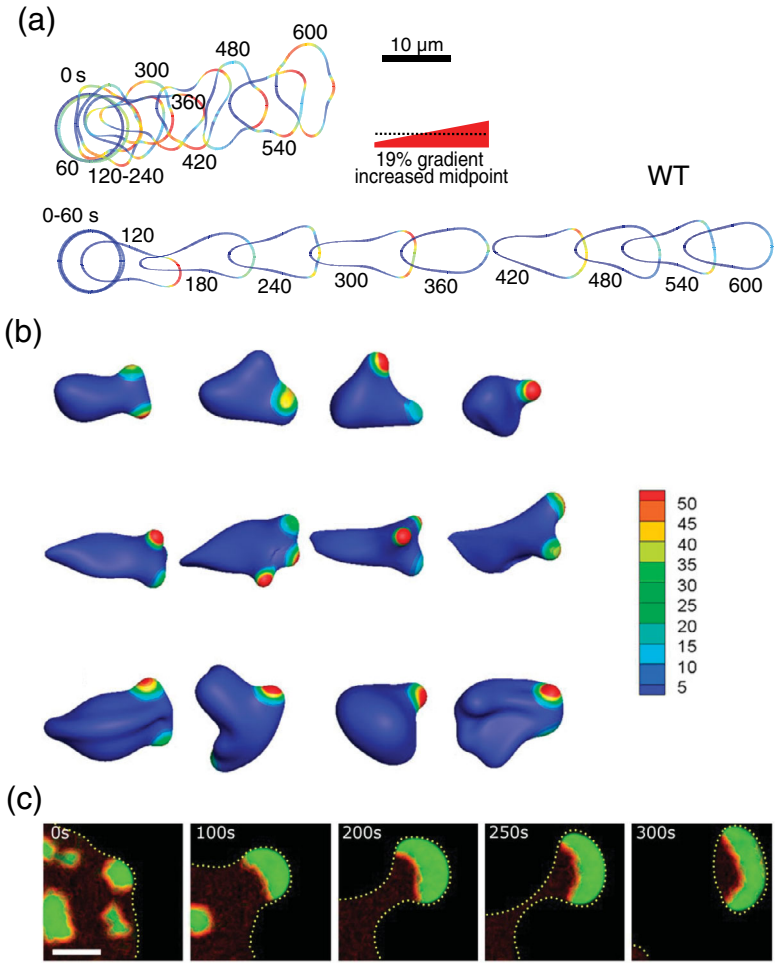

FIGURE 5 Cell migration. (a) Simulations of cell chemotactic movement using the LSM. This simulation compares the movement of a cell without (top) or with (bottom) an adaptation mechanism in response to a chemoattractant gradient. The color along the perimeter represents the activity of the species that regulates protrusive forces (Reprinted from Shi et al. (2013) with permission under the Creative Commons Attribution License). (b) Simulation of 3D cell migration using the IBM. Shown are instantaneous cell shapes at varying membrane stiffness viscosity ratios. The cells swim from left to right. Color bar represents activator concentration (Reprinted with permission from Campbell and Bagchi (2017). Copyright 2017 AIP Publishing). (c). Simulations of wave dynamics in giant *Dictyostelium* cells. As the wave of activity reaches the cell perimeter, it pushes the boundary eventually driving the cell to cytofission. The fragments then move in a highly persistent fashion (Reprinted from Flemming, Font, Alonso, and Beta (2020) with permission of the authors)

showed that these modes could be generated by varying mechanical parameters. Importantly, Zhan et al. (2020) have recently shown that similar alterations can be effected to drive actin-based protrusions in human epithelial cells and that the resulting wave activity was progressively enhanced across a series of increasingly metastatic breast cancer cell lines.

In a recent model using the PFM, Flemming et al. (2020) showed how actin waves that arise from the excitable system can drive the cell to divide. Their simulations, which are supported by experiments on giant *Dictyostelium* cells obtained by electrofusion and exhibiting high activity levels because of a deletion of a RasGAP, show that collision of the waves with the cell boundary push the membrane outward. Moreover, these protrusions can lead to the formation of small fan-shaped enucleated cells that exhibit highly persistent motion (Figure 5c).

4.1.3 | Relationship with ECM and durotaxis

The chemical cues presented by the ECM are key determinants for both development and cancer progression (Walker, Mojares, & Del Río Hernández, 2018). Moreover, many cells, including cancer cells, display *durotaxis*, directed cell migration in response to changes in the substrate stiffness which has recently been shown to drive cancer cell migration (DuChez, Doyle, Dimitriadis, & Yamada, 2019; Lo, Wang, Dembo, & Wang, 2000). This has prompted a number of mechano-biochemical models of cell migration to consider the interaction of cells with the ECM.

Zhu and Mogilner (2016) modeled a cell consisting of a dynamic actin-myosin network surrounding a rigid nucleus and enclosed by an elastic membrane. The ECM was represented by a spring network. Their simulations reproduced five modes of motility if they were able to include or exclude proteolysis, and vary adhesion, protrusion, contraction, and adhesion. Heck et al. (2020) recently developed a 2D computational model of cell migration through a degradable viscoelastic ECM and used it to show that changes in ECM stiffness and cell strength affect cell migration and are

accompanied by changes in number, lifetime, and length of protrusions. Moreover, though force-dependent adhesion disassembly did not lead to faster migration, it could increase its efficiency. Using a 3D model, Kim et al. (2018) studied how filopodia sense ECM stiffness. The model was tested by simulating cell movement across regions of ECM of different mechanical properties and showed that cells migrated towards stiffer regions.

Marzban, Kang, Li, Sun, and Yuan (2019) coupled a biochemical model consisting of reaction–diffusion equations of protrusive and contractile signals with a mechanical model that includes cell–substrate interaction to study cell motion. Their simulations were evaluated by comparing to traction-force microscopy measurements. Simulations of cell motion between regions of varying rigidity showed cells turning at the stiff-to-soft interphase followed by crawling along boundary. These turns were caused by a positive feedback in which larger substrate stiffness leads to larger traction stress, greater focal adhesion and a higher protrusive activity. Escribano et al. (2018) also considered durotaxis in the context of collected cell migration. Their model showed that collective durotaxis is more efficient than that of single cells. Moreover, they demonstrated that this is due to the fact that collectively, cells are able to deform the substrate in regions with lower stiffness more than single cells.

Whereas these models consider substrate of spatially varying rigidity, Molina and Yamamoto (2019) simulated the motion of keratocyte-like cells on cyclically stretched substrates. They showed that the cellular axis could be realigned, or could display bistable orientation, depend on the type of coupling with the substrate.

4.2 | Collective cell migration

While most studies of cell migration have concentrated on the movement of single cells, these models are now being extended to consider multicellular interactions. This is particularly important as various physiological functions, such as wound healing and cancer metastases, depend on the coordinated movement of groups of cells (Friedl & Gilmour, 2009).

Yang and Levine (2018) relied on a simple particle-based model of cells including purse-string contraction and cell crawling to study epithelial wound healing. Within this model, each cell consists of two subcellular compartments, one representing the front end of the cell, the other the back end (Zimmermann, Camley, Rappel, & Levine, 2016). Through a series of articles, Camley and coworkers have studied the role of collective chemotaxis. Using this same two-compartment model, they analyzed a collective version of the LEGI mechanism (Camley, Zimmermann, Levine, & Rappel, 2016). Similar results using a CPM model were obtained by Varennes, Han, and Mugler (2016). Camley and Rappel (2017) also studied how heterogeneity in the mechanical properties and biochemical response of cells within the cluster affects collective chemotaxis.

Nonomura (2012) considered 2D clusters of cells using the PFM, taking into account cell adhesion and excluded volume. Their model included cell adhesion, rearrangement of a cell cluster, chemotaxis, and cell sorting, as well as the three-dimensional results of cell clusters. These cells, however, were stationary. More realistic models have been considered. Camley et al. (2014) used a PFM model of cell motility to consider the interaction of two motile cells, but also included reaction–diffusion equations to consider Rho GTPases as a driver of cell motility. They showed that rotational motility was regulated by cell polarity. Kulawiak et al. (2016) also considered colliding pairs of cells and recreated the variety of results seen experimentally, including the reversal of polarity upon contact, sticking, and migrating past each other.

Löber et al. (2015) expanded the PFM model of Ziebert and Aranson (2013) to account for multiple cells. In this case, each cell is described by a phase-field function, and their interactions are penalized by introducing an energy functional that penalizes the overlap of the two functions. Their simulations showed that collective migration arose from inelastic collisions between neighboring cells. These collisions led to alignment of the cells and clusters of cells that moved together. This could be reduced by lowering the adhesion coefficient. Figure 6a shows the result of one of their simulations in which cells migrated within a confined, circular domain. Note that the cells organize to rotate collectively. Najem and Grant (2016) also used a PFM incorporating adhesion, surface tension, repulsion, attraction, and polarization and showed that cells could align to form tissue-like sheets of cells.

4.3 | Cytokinesis

Cytokinesis is the final stage of cell division during which one mother cell divides and gives rise to two daughter cells. This process requires significant cell shape change and the coordination of the complex physical machinery within the

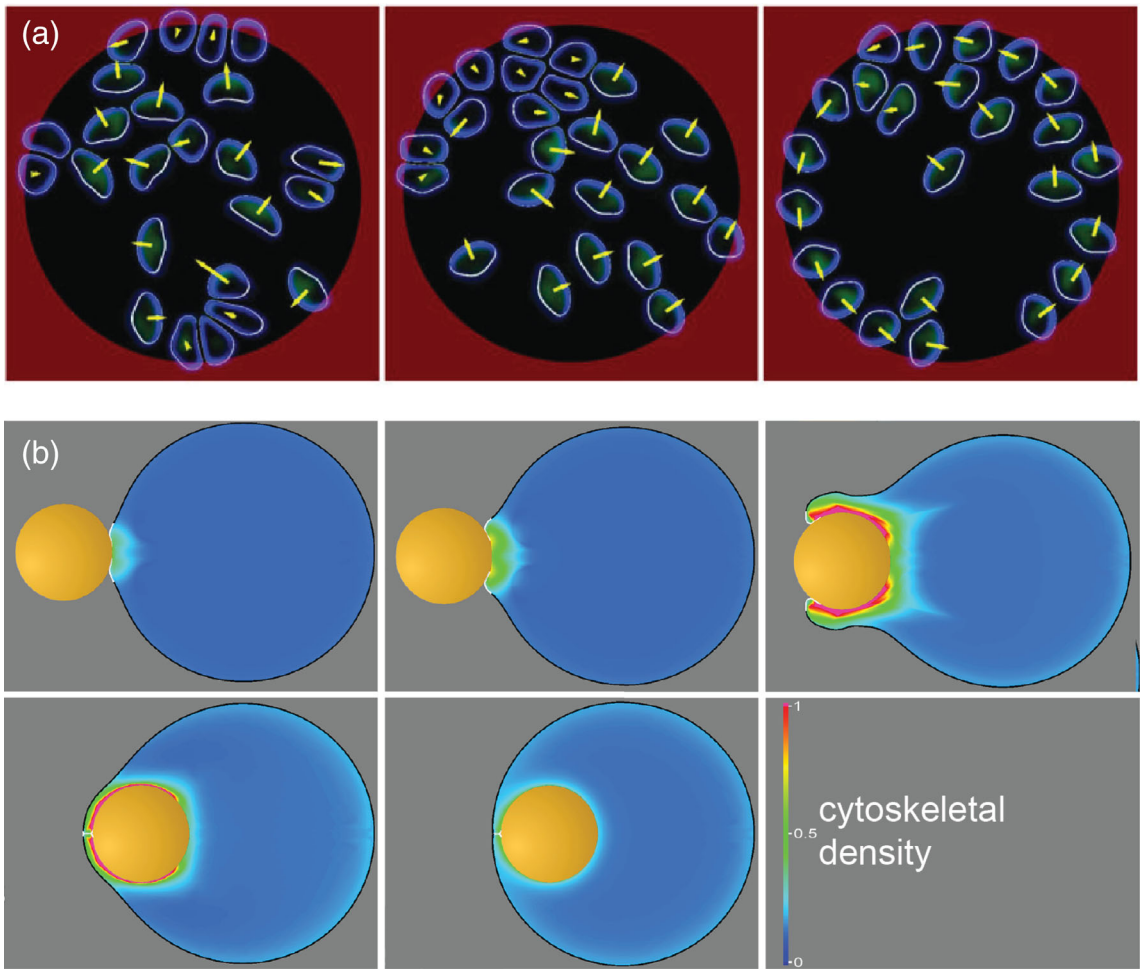

FIGURE 6 Cell shape changes. (a) Simulation of collective cell migration using PFM. The cells are restricted to moving inside the circle. As a result, the cells organize to move radially (Reprinted from Löber et al. (2015) with permission under a Creative Commons Attribution 4.0 International License). (b) Phagocytosis simulation. Snapshots of simulations of the engulfment of antibody-coated beads (Reprinted from Herant, Lee, Dembo, and Heinrich (2011) with permission under a Creative Commons Attribution License). Note that the individual panels have been rearranged to fit the page better

cell. Owing to the inherent complexity of cytokinesis, computational models can assist in deciphering the mechanistic details that may be difficult to uncover experimentally.

At a fundamental level, a cell can be considered to behave like a water droplet with motion that can be dominated by surface tension and curvature. The ingression of the cleavage furrow between the dividing cells drives the final phase of cell division. The dynamics of the progression of the furrow cleavage is important for determining the success of a cell division event (Nguyen & Robinson, 2020; Pollard & O'Shaughnessy, 2019; Zhang & Robinson, 2005). Using LSM and a viscoelastic mechanical model based on experimentally measured parameters, Poirier et al. (2012) described different phases of cell division, including the dynamics of the furrow cleavage (Figure 7a). They showed that either the contractile stress of myosin II or protrusive forces on the poles was sufficient for furrow cleavage formation. In the second phase of cell division, passive Laplace-like forces, which are derived from cortical tension and surface curvature, are sufficient to complete division. This model was able to recreate quantitatively various modes of cell division including traction-mediated cytofission and myosin-independent cytokinesis seen in *Dictyostelium* cells.

The symmetrical nature of cytokinesis makes it a desirable target for building models in three dimensions. Li and Kim (2016) made significant advancements to mathematical methodology of 3D simulations using the IBM (Figure 7b). They implemented a fully 3D model of cell division including a novel remeshing algorithm to prevent surface distortions and a volume conservation algorithm to maintain cell size. Their mathematical system provides a computational foundation upon which more biological elements can be added to capture the complexity of cell division fully. Similarly, Zhao and Wang (2016a, 2016b) modeled a dividing cell as a hydrodynamic system and implemented it using a 3D

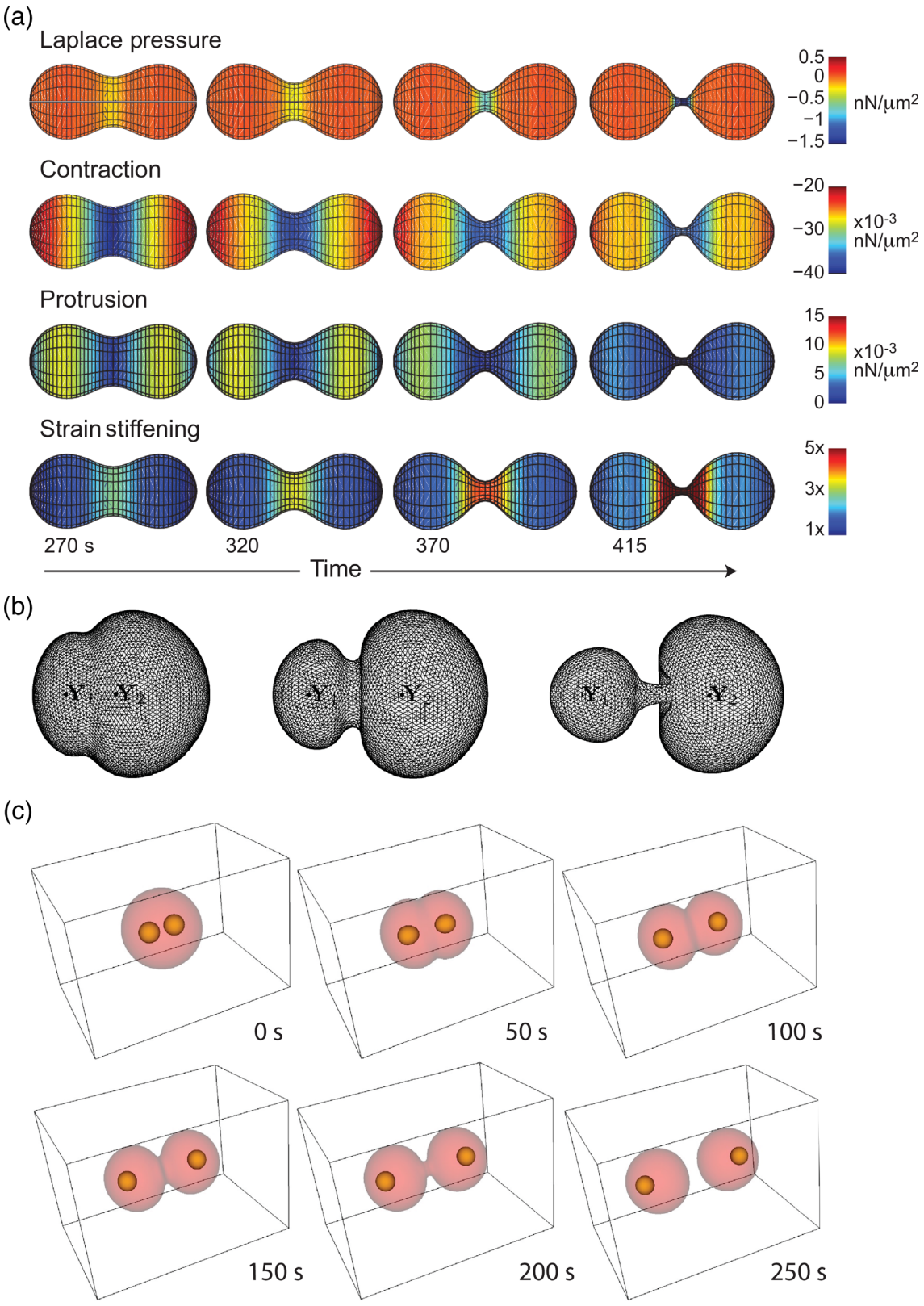

FIGURE 7 Simulations of cell division. (a) Simulation of cytokinesis using the LSM. The four rows depict the relative contribution of each force to during time (Reprinted from Poirier et al. (2012) with permission under the Creative Commons Attribution License). (b) Three-dimensional IBM simulation of asymmetric cell division. The asymmetry is obtained by specifying varying positions for the asters, marked by the letter "Y" (Reprinted with permission from Li and Kim (2016). Copyright 2015 Elsevier Inc.). (c) Simulation of cytokinesis using PFM. These simulations show the nucleus (yellow spheres) surrounded by the cytoplasm. After splitting, the daughter cells round up under the influence of surface tension (Reprinted with permission from Zhao and Wang (2016b). Copyright © John Wiley & Sons, Ltd.)

PFM. They included an actomyosin contractile system on the cell cortex and a cytokinetic ring. The force acting on the cell was assumed to be proportional to the concentration of actomyosin and the surface tension at any given point. The results of their model qualitatively agree with many experimental observations. As seen in Figure 7c, these simulations show one advantage of implicit boundary schemes such as the PFM and LSM, in that changes in topology, such as when the mother cell gives rise to two independent daughter cells.

Looking more closely at the organization of the cytoskeleton at the cleavage furrow specifically, Minc, Burgess, and Chang (2011), through a combination of experimental and agent based modeling, determined how the mitotic spindles were positioned, ultimately determining the placement of the furrow cleavage. They found that dynein motor proteins that are positioned in the cytoplasm and on the cell cortex create a force balance by pulling on astral microtubules which places the spindle in the correct position.

To understand the complex structure that allows this force balance to occur, Vavylonis, Wu, Hao, O'Shaughnessy, and Pollard (2008) used an ABM approach to describe the self-assembly of the cytoskeletal agents that make up the contractile machinery, including random search, capture, pull, release mechanism of actin filaments and myosins. They showed how a stable ring structure was formed within the appropriate biological time scale. Their model recapitulated classic cytokinesis experiments including ring fusion events. They hypothesized that even though the model did not include all potential cytoskeletal cross linkers and regulatory proteins, the randomness allowed sufficient plasticity of the system to capture the biological event.

4.4 | Mechanosensation and mechanotransduction

Cells live in complex and varied environments. For the cell to respond appropriately to the stressors it will experience in its surroundings, it must be capable of sensing and responding to the signals it is receiving. This process, known as *mechanosensation* and *mechanotransduction* is implicated in cellular signaling, transcriptional events, cellular memory, and cytoskeletal architecture. When a cell's ability to sense and respond to its environment is disrupted, aberrant cell shape and cell motility often ensue leading to disease states (Surcel & Robinson, 2019).

Sensation of substrate stiffness is important in a cell's ability to migrate and proliferate appropriately, among other things (Janmey, Fletcher, & Reinhart-King, 2020). Depending on the stiffness of the substrate, a cell may need more or less adhesion molecules to complete the desired biological process. Identifying which parts of molecular basis by which cells can sense this stiffness can be difficult to explore experimentally. Computational and mathematical models allow for minimal cells to be built in silico and systematically tested to identify the most robust features of mechanosensation which could then become targets for disease treatments.

At a molecular level, Borau, Kim, Bidone, García-Aznar, and Kamm (2012) explored the role of actomyosin systems in substrate sensing using a 3D ABM using Brownian dynamics to simulate molecular movements. The model included an actin meshwork (actin crosslinking proteins, actin filaments) and motor proteins which could bind to the actin. The motors would act on the actin filaments, moving pairs of F-actin fibers in a polar fashion. The density of the actin meshwork could be altered to represent different substrate or ECM stiffnesses. They determined that there was a biphasic relationship between the stiffness of the substrate and the amount of stress on the system. On stiff substrates (highly heterogeneous, less compressed actin meshwork), the motors reach a maximum force production leading to stalling and high stress. In contrast, on soft substrates (more compressed actin meshwork), motor proteins are limited by steric interactions with the actin meshwork and other motor proteins. This study showed that the actomyosin contractility system alone is sufficient to sense substrate stiffness.

Looking specifically at the adhesion molecules between a cell and its surrounding substrate, Oakes et al. (2018) used a biophysical model to explore the role of integrin–fibronectin bonds in mechanosensation. Using a mathematical approach, they parsed out which parts of adhesion bond kinetics were most important for stiffness sensing. The integrin–ECM bonds were modeled as a catch bond meaning the bond lifetime is a function of applied mechanical load. They found that this property of the bond was required for mechanosensation and the cell's ability to sense substrate stiffness. If this property was removed, the cell was unable to sense the stiffness of the substrate. They also found that these bonds were optimized to sense changes in matrix stiffness with a Young's modulus of 6 kPa or higher which is consistent with experimental findings.

Zhang et al. (2020) studied the impact of altered substrate stiffness (caused either by the cell applying contractile forces to the substrate, or an external force being applied to the substrate) on cell shape change, ultimately leading to altered cellular migration. Using the LSM, they modeled fish epidermal keratocytes on elastic substrates of differing

stiffnesses. Their model recapitulated several biological processes such as the required symmetry-breaking from a stationary centrosymmetric keratocyte to a migrating crescent keratocyte. Additionally, the model demonstrated a new symmetry-breaking mechanism. Specifically, they posited that when a cell applies force to a substrate the resulting force depends on the local shape of the cell. However, the cell's shape is dictated by the substrate stress. This feedback loop explained protrusive and contractile mechanisms that led to the polarity required for cellular migration.

4.5 | Cell-in-cell events

Cell engulfment, or cell-in-cell events are often seen throughout biology, and are particularly important in the context of cancer. Metastatic cancers are often correlated with high frequency of cell-in-cell events (Fais & Overholtzer, 2018). This process, also known as *entosis*, is characterized by a population of cells with mechanical heterogeneity and all cells expressing E-cadherin (Overholtzer et al., 2007; Sun et al., 2014). The more mechanically deformable cells (so-called *winners*) engulf the less mechanically deformable cells (*losers*) and break the loser cells down as a source of nutrients. Because of the competition for nutrients in many cancers and the potential for high degrees of mechanical heterogeneity, entotic events are often upregulated. Through computational simulations based on measured experimental parameters, Sun et al. (2014) determined that a difference in myosin contractility between the winner and loser cells made completion of entotic events more energetically favorable thus allowing entosis to proceed spontaneously. Inclusion of actomyosin contractility, especially on the loser cell is therefore critical to successful entotic events.

Though entosis is seen where cells of the same type cannibalize each other, cells can also engulf bacteria and other particles that are typically smaller than themselves during phagocytosis. Defects in phagocytes (neutrophils, monocytes, etc.), particularly in patients who have other underlying health conditions, can lead to increased risk of infections and other diseases and ultimately increasing risk of mortality (Engelich, Wright, & Hartshorn, 2001). In a series of articles, Herant, Heinrich, and Dembo (2005, 2006) and Herant et al. (2011) developed a finite element model of phagocytosis using "reactive interpenetrating flow" formalism. In their model, they challenged neutrophils with the fungal particle zymosan. They adapted their prior models of engulfment of antibody-coated beads to represent more accurately the engulfment of a live biological particle (Figure 6b). Their current model includes both adhesion between the neutrophil and the zymosan, and force production in the neutrophil via a generic cytoskeletal signaling pathway to model action polymerization. The resulting adhesion and action polymerization on either side of the nascent adhesion results in a transient increase in both cortical tension and cytoplasmic viscosity. Using their prior model alongside this model, the authors determined the mechanical differences in the antibody-coated bead engulfment and the zymosan engulfment. Contrasting the engulfment of the fungi (described above), phagocytosis of a coated bead resulted in tight cell-target adhesion which limited the protrusions of the neutrophils to areas that were not adhered to the bead.

Looking more closely at what drives adhesion bond formation between a phagocyte and a target, Tollis, Dart, Tzircotis, and Endres (2010) developed a 3D stochastic biophysical model implemented using an opensource finite element simulation software, Surface Evolver (Brakke, 1992). They then used a Monte Carlo algorithm to implement the thermal fluctuations and active membrane deformations. The particle is engulfed using a zipper-like mechanism driven by the ratcheting motion of the cell membrane. They explore the contributions of passive Brownian motion verses active actin polymerization to determine what is necessary to drive a successful phagocytic event. The authors found that in the absence of active actin polymerization, cells were able to complete phagocytosis with purely Brownian fluctuations for particles with radii less than 2.5 μm (though the engulfment took longer to complete compared to active zippering). The increased efficiency in the presence of actin polymerization was argued to reinforce the membrane deformations caused by the thermal motion resulting in irreversible adhesion formation.

5 | DISCUSSION AND OUTLOOK

To unravel the nature of a diseased system ultimately requires that we understand how cells maintain a healthy state. A cell's survival and proper function rely on its ability to control their shape though sensing and responding to their environment. Cells gain significant insight about their surroundings through mechanosensation. This sensing effects cell signaling that leads to changes in migration, adhesion, and division. If any one of these processes goes awry, it can lead to various disease states in the system. Uncontrolled cell growth, abnormal cell migration, and inappropriate signaling resulting from improper mechanical transduction are often correlated with cancerous systems. Similarly, if a cell

TABLE 1 Continuum description of mechanics

Biological problem	Method	Dim.	References
Actin polymer dynamics	ABM	2D	Bidone et al. (2017)
	Biophysical	2D	Chanet et al. (2017)
Cell migration	CPM	2D	Niculescu et al. (2015)
	FEM	2D	Arefi et al. (2020), Neilson et al. (2011)
		3D	Kim et al. (2018)
	IBM	2D	Bottino (1998, 2001), Bottino et al. (2002), Vanderlei et al. (2011)
		3D	Campbell and Bagchi (2017, 2018)
	PFM	2D	Alonso et al. (2018), Bresler et al. (2019), Camley et al. (2014), Kulawiak et al. (2016), Löber et al. (2015), Molina and Yamamoto (2019), Moure and Gomez (2020a, 2020b), Shao et al. (2010, 2012), Tao et al. (2020), Ziebert and Aranson (2013)
		3D	Moure and Gomez (2018), Cao et al. (2019)
	LSM	2D	Yang et al. (2008)
Collective cell migration	CPM	2D	Thüroff, Goychuk, Reiter, and Frey (2019)
	PFM	2D	Yang, Jolly, and Levine (2019)
Cytokinesis	ABM	2D	Minc et al. (2011), Vavylonis et al. (2008), Cortes et al. (2020)
	IBM	2D	Bächer and Gekle (2019)
		3D	Lee (2018), Li and Kim (2016)
	LSM	2D	Poirier et al. (2012)
	PFM	3D	Zhao and Wang (2016a, 2016b)
Mechanosensation	ABM	3D	Borau et al. (2012)
	LSM	2D	Zhang et al. (2020)
	FEM	3D	Ganesh et al. (2020)
Phagocytosis	FEM	2D	Herant et al. (2011)
Wound healing	FEM	2D	Escribano et al. (2018)
	LSM	2D	Ben Amar and Wu (2014)
Entosis		1D	Sun et al. (2014)
Growth	LSM	3D	Alias and Buenzli (2020)

is unable to locate and migrate appropriately towards targets, it can lead to immunodeficiencies and increased risk of infection.

Looking at the numerous techniques that have been described above (Table 1), a reader seeking some guidance as to how to start a modeling effort might feel somewhat overwhelmed. What method to use? Hopefully, this review has shown that the particular method chosen is not paramount—different modeling simulation methodologies can give rise to quite similar results. The advice we can offer here is based on our personal experience. Approximately 15 years ago, we were in a similar situation, having developed a number of biochemical models of cell gradient sensing (Levchenko & Iglesias, 2002; Ma, Janetopoulos, Yang, Devreotes, & Iglesias, 2004) and division/mechanosensation (Effler et al., 2006; Zhang & Robinson, 2005) but wished to investigate whether these models could recreate realistic cell shape changes. Our expertise was neither in mechanics nor in numerical methods. We considered several methodologies (IBM, FEM) but were quickly overwhelmed by the complexity of the simulations, primarily because of a dearth of easy-to-use software. On the other hand, after discovering the LSM Matlab toolbox (Mitchell, 2008), we were able to start implementing models of shape changes within a couple of weeks. We were aided by the fact that our lab members were well versed on the underlying software and the package was well documented. In our experience, this overcame the hurdles in front of us and allowed us to concentrate on answering the biological questions that interested us. Were we starting again now, the answer might have been different as the availability of software tools has increased and there is now plenty of expertise as documented in the papers reviewed here. However, we still

believe that there is still a large need for the development of more user-friendly software in a number of programing environments.

Computational techniques like the ones described here can help elucidate the details of the mechanisms that drive cell shape change. A little over a century ago, D'Arcy Thompson (1917) wrote:

> If we look at the living cell of an Amoeba or a Spirogyra, we see a something which exhibits certain active movements, and a certain fluctuating, or more or less lasting, form; and its form at a given moment, just like its motions, is to be investigated by the help of physical methods, and explained by the invocation of the mathematical conception of force.

While looking over the results reviewed here, it is remarkable how prescient these words were. As our understanding of the role of mechanics and cell shape in disease increases, there is no doubt that the role of mathematics and computation will only grow. From our survey of the methods that have been used, it is not clear that there is a technique that has a clear advantage over the others. On a purely technical level, one of the biggest hurdles is the availability of simulation platforms that are easy to use and accessible to the non-expert. Though they have become more common, open source, adaptable software will be of importance to continue to move the field forward. The ability to tie these simulations to experiments and experimentally obtained data will also be important.

Moreover, importantly, because of the wide range of tools needed to understand these processes, a largely interdisciplinary approach is needed: biologists to ground the work, provide its context, and to carry out the experiments that are the ultimate test of the theory; engineers and physicists for the physical description of matter; systems and control engineers for their insight into regulation; and mathematicians and computer scientists for the algorithmic tools that enable conceptual tools to be tested in silico. Over the last 20 years, the presence of these interdisciplinary teams has grown tremendously, but there is room for more. Previously we argued that a critical step to a successful interdisciplinary collaboration is a commitment to learn each other's scientific languages (Robinson & Iglesias, 2012). This is still true today.

ACKNOWLEDGMENTS

The authors thank the members of the Iglesias and Robinson labs for their comments on the manuscript. We have also benefited for years with discussions with Peter Devreotes and lab members. Our work in this field has been supported by DARPA, HR0011-16-C-0139 and the NIH grant GM66817 (DNR).

CONFLICT OF INTEREST

The authors have declared no conflicts of interest for this article..

AUTHOR CONTRIBUTIONS

Kathleen DiNapoli: Visualization; writing-original draft; writing-review and editing. **Douglas Robinson:** Writing-original draft; writing-review and editing. **Pablo Iglesias:** Visualization; writing-original draft; writing-review and editing.

ORCID

Pablo A. Iglesias https://orcid.org/0000-0002-0840-155X

RELATED WIREs ARTICLES

Tuneable resolution as a systems biology approach for multi-scale, multi-compartment computational models
Modeling, signaling and cytoskeleton dynamics: integrated modeling-experimental frameworks in cell migration
Computational modeling of single-cell mechanics and cytoskeletal mechanobiology
Stochastic simulation algorithms for computational systems biology: Exact, approximate, and hybrid methods
Computational models to explore the complexity of the epithelial to mesenchymal transition in cancer

FURTHER READING

Camley, B. A., & Rappel, W.-J. (2017). Physical models of collective cell motility: From cell to tissue. Journal of Physics D: Applied Physics, 50(11), 113002.

Cheng, B., Lin, M., Huang, G., Li, Y., Ji, B., Genin, G. M., ... Xu, F. (2017). Cellular mechanosensing of the biophysical microenvironment: A review of mathematical models of biophysical regulation of cell responses. Physics of Life Reviews, 22–23, 88–119.

Cortes, D. B., Dawes, A., Liu, J., Nickaeen, M., Strychalski, W., & Maddox, A. S. (2018). Unite to divide – How models and biological experimentation have come together to reveal mechanisms of cytokinesis. Journal of Cell Science, 131(24), jcs203570.

Norden, C., & Lecaudey, V. (2019). Collective cell migration: General themes and new paradigms. Current Opinion in Genetics and Development, 57, 54–60.

Richards, D. M., & Endres, R. G. (2017). How cells engulf: A review of theoretical approaches to phagocytosis. Reports on Progress in Physics, 80(12), 126601.

Vorselen, D., Labitigan, R. L. D., & Theriot, J. A. (2020). A mechanical perspective on phagocytic cup formation. Current Opinion in Cell Biology, 66, 112–122.

Wan, L., Neumann, C. A., & LeDuc, P. R. (2020). Tumor-on-a-chip for integrating a 3D tumor microenvironment: Chemical and mechanical factors. Lab on a Chip, 20, 873–888.

REFERENCES

Adalsteinsson, D., & Sethian, J. (2003). Transport and diffusion of material quantities on propagating interfaces via level set methods. *Journal of Computational Physics*, *185*(1), 271–288.

Adalsteinsson, D., & Sethian, J. A. (1995). A fast level set method for propagating interfaces. *Journal of Computational Physics*, *118*(2), 269–277.

Alias, M. A., & Buenzli, P. R. (2020). A level-set method for the evolution of cells and tissue during curvature-controlled growth. *International Jorunal of Numerical Methods in Biomedical Engineering*, *36*(1), e3279.

Almendro-Vedia, V. G., Monroy, F., & Cao, F. J. (2013). Mechanics of constriction during cell division: A variational approach. *PLoS One*, *8* (8), e69750.

Alonso, S., Stange, M., & Beta, C. (2018). Modeling random crawling, membrane deformation and intracellular polarity of motile amoeboid cells. *PLoS One*, *13*(8), e0201977.

Andrews, S. S. (2012). Spatial and stochastic cellular modeling with the Smoldyn simulator. *Methods in Molecular Biology*, *804*, 519–542.

Arefi, S. M. A., Tsvirkun, D., Verdier, C., & Feng, J. J. (2020). A biomechanical model for the transendothelial migration of cancer cells. *Physical Biology*, *17*(3), 036004.

Arjunan, S. N. V., Miyauchi, A., Iwamoto, K., & Takahashi, K. (2020). Pspatiocyte: A high-performance simulator for intracellular reaction-diffusion systems. *BMC Bioinformatics*, *21*(1), 33.

Bächer, C., & Gekle, S. (2019). Computational modeling of active deformable membranes embedded in three-dimensional flows. *Physical Review E*, *99*, 062418.

Bansod, Y. D., Matsumoto, T., Nagayama, K., & Bursa, J. (2018). A finite element bendo-tensegrity model of eukaryotic cell. *Journal of Biomechanical Engineering*, *140*(10), 101001.

Barrett, J. W., Garcke, H., & Nürnberg, R. (2007). A parametric finite element method for fourth order geometric evolution equations. *Journal of Computational Physics*, *222*(1), 441–467.

Battista, N. A., Strickland, W. C., & Miller, L. A. (2017). Ib2d: A Python and Matlab implementation of the immersed boundary method. *Bioinspiration & Biomimetics*, *12*(3), 036003.

Bellas, E., & Chen, C. S. (2014). Forms, forces, and stem cell fate. *Current Opinion in Cell Biology*, *31*, 92–97.

Bellotti, T., & Theillard, M. (2019). A coupled level-set and reference map method for interface representation with applications to two-phase flows simulation. *Journal of Computational Physics*, *392*, 266–290.

Ben Amar, M., & Wu, M. (2014). Re-epithelialization: Advancing epithelium frontier during wound healing. *Journal of the Royal Society Interface*, *11*(93), 20131038.

Berg, H. C. (1993). *Random walks in biology* (expanded ed.). Princeton, NJ: Princeton University Press.

Biben, T., Kassner, K., & Misbah, C. (2005). Phase-field approach to three-dimensional vesicle dynamics. *Physical Review E: Statistical, Nonlinear, and Soft Matter Physics*, *72*(4 Pt 1), 041921.

Biben, T., & Misbah, C. (2003). Tumbling of vesicles under shear flow within an advected-field approach. *Physical Review E: Statistical, Nonlinear, and Soft Matter Physics*, *67*(3 Pt 1), 031908.

Bidhendi, A. J., & Geitmann, A. (2018). Finite element modeling of shape changes in plant cells. *Plant Physiology*, *176*(1), 41–56.

Bidone, T. C., Jung, W., Maruri, D., Borau, C., Kamm, R. D., & Kim, T. (2017). Morphological transformation and force generation of active cytoskeletal networks. *PLoS Computational Biology*, *13*(1), e1005277.

Borau, C., Kim, T., Bidone, T., García-Aznar, J. M., & Kamm, R. D. (2012). Dynamic mechanisms of cell rigidity sensing: Insights from a computational model of actomyosin networks. *PLoS One*, *7*(11), e49174.

Bosgraaf, L., & Van Haastert, P. J. M. (2009). The ordered extension of pseudopodia by amoeboid cells in the absence of external cues. *PLoS One*, *4*(4), e5253.

Bottino, D., Mogilner, A., Roberts, T., Stewart, M., & Oster, G. (2002). How nematode sperm crawl. *Journal of Cell Science*, *115*(Pt 2), 367–384.

Bottino, D. C. (1998). Modeling viscoelastic networks and cell deformation in the context of the immersed boundary method. *Journal of Computational Physics*, *147*(1), 86–113.

Bottino, D. C. (2001). Computer simulations of mechanochemical coupling in a deforming domain: Applications to cell motion. In P. K. Maini & H. G. Othmer (Eds.), *Mathematical models for biological pattern formation* (pp. 295–314). New York, NY: Springer New York.

Brakke, K. A. (1992). The surface evolver. *Experimental Mathematics*, *1*(2), 141–165.

Bresler, Y., Palmieri, B., & Grant, M. (2019). Sharp interface model for elastic motile cells. *The European Physical Journal E: Soft Matter*, *42*(5), 52.

Brill-Karniely, Y., Nisenholz, N., Rajendran, K., Dang, Q., Krishnan, R., & Zemel, A. (2014). Dynamics of cell area and force during spreading. *Biophysical Journal*, *107*(12), L37–L40.

Cahn, J. W., & Hilliard, J. E. (1958). Free energy of a nonuniform system. I. Interfacial free energy. *Journal of Chemical Physics*, *258*(2), 258–267.

Camley, B. A., & Rappel, W.-J. (2017). Cell-to-cell variation sets a tissue-rheology-dependent bound on collective gradient sensing. *Proceedings of the National Academy of Sciences of the United States of America*, *114*(47), E10074–E10082.

Camley, B. A., Zhang, Y., Zhao, Y., Li, B., Ben-Jacob, E., Levine, H., & Rappel, W.-J. (2014). Polarity mechanisms such as contact inhibition of locomotion regulate persistent rotational motion of mammalian cells on micropatterns. *Proceedings of the National Academy of Sciences of the United States of America*, *111*(41), 14770–14775.

Camley, B. A., Zimmermann, J., Levine, H., & Rappel, W.-J. (2016). Collective signal processing in cluster chemotaxis: Roles of adaptation, amplification, and co-attraction in collective guidance. *PLoS Computational Biology*, *12*(7), e1005008.

Campbell, E. J., & Bagchi, P. (2017). A computational model of amoeboid cell swimming. *Physics of Fluids*, *29*(10), 101902.

Campbell, E. J., & Bagchi, P. (2018). A computational model of amoeboid cell motility in the presence of obstacles. *Soft Matter*, *14*(28), 5741–5763.

Cao, Y., Ghabache, E., Miao, Y., Niman, C., Hakozaki, H., Reck-Peterson, S. L., ... Rappel, W.-J. (2019). A minimal computational model for three-dimensional cell migration. *Journal of Royal Society Interface*, *16*(161), 20190619.

Chanet, S., Miller, C. J., Vaishnav, E. D., Ermentrout, B., Davidson, L. A., & Martin, A. C. (2017). Actomyosin meshwork mechanosensing enables tissue shape to orient cell force. *Nature Communications*, *8*, 15014.

Cortes, D. B., Gordon, M., Nédélec, F., & Maddox, A. S. (2020). Bond type and discretization of nonmuscle myosin II are critical for simulated contractile dynamics. *Biophysical Journal*, *118*(11), 2703–2717.

Cowan, A. E., Moraru, I. I., Schaff, J. C., Slepchenko, B. M., & Loew, L. M. (2012). Spatial modeling of cell signaling networks. *Methods in Cell Biology*, *110*, 195–221.

Cross, S. E., Jin, Y.-S., Rao, J., & Gimzewski, J. K. (2007). Nanomechanical analysis of cells from cancer patients. *Nature Nanotechnology*, *2*(12), 780–783.

Devreotes, P. N., Bhattacharya, S., Edwards, M., Iglesias, P. A., Lampert, T., & Miao, Y. (2017). Excitable signal transduction networks in directed cell migration. *Annual Review of Cell and Developmental Biology*, *33*, 103–125.

Dhatt, G., Touzot, G., & Lefrançois, E. (2012). Finite element method. In *Numerical methods series*. London: ISTE.

Dillon, R., & Othmer, H. G. (1999). A mathematical model for outgrowth and spatial patterning of the vertebrate limb bud. *Journal of Theoretical Biology*, *197*(3), 295–330.

Drawert, B., Engblom, S., & Hellander, A. (2012). Urdme: A modular framework for stochastic simulation of reaction-transport processes in complex geometries. *BMC Systems Biology*, *6*(1), 76.

Du, Q., Liu, C., & Wang, X. (2004). A phase field approach in the numerical study of the elastic bending energy for vesicle membranes. *Journal of Computational Physics*, *198*(2), 450–468.

DuChez, B. J., Doyle, A. D., Dimitriadis, E. K., & Yamada, K. M. (2019). Durotaxis by human cancer cells. *Biophysical Journal*, *116*(4), 670–683.

Effler, J. C., Kee, Y.-S., Berk, J. M., Tran, M. N., Iglesias, P. A., & Robinson, D. N. (2006). Mitosis-specific mechanosensing and contractile-protein redistribution control cell shape. *Current Biology*, *16*(19), 1962–1967.

Elgeti, S., & Sauerland, H. (2016). Deforming fluid domains within the finite element method: Five mesh-based tracking methods in comparison. *Archives of Computational Methods in Engineering*, *23*(2), 323–361.

Elliott, C. M., Stinner, B., & Venkataraman, C. (2012). Modelling cell motility and chemotaxis with evolving surface finite elements. *Journal of Royal Society Interface*, *9*(76), 3027–3044.

Engelich, G., Wright, D. G., & Hartshorn, K. L. (2001). Acquired disorders of phagocyte function complicating medical and surgical illnesses. *Clinical Infectious Diseases*, *33*(12), 2040–2048.

Escribano, J., Sunyer, R., Sánchez, M. T., Trepat, X., Roca-Cusachs, P., & García-Aznar, J. M. (2018). A hybrid computational model for collective cell durotaxis. *Biomechanics and Modeling in Mechanobiology*, *17*(4), 1037–1052.

Fais, S., & Overholtzer, M. (2018). Cell-in-cell phenomena in cancer. *Nature Reviews. Cancer*, *18*(12), 758–766.

Flemming, S., Font, F., Alonso, S., & Beta, C. (2020). How cortical waves drive fission of motile cells. *Proceedings of the National Academy of Sciences of the United States of America*, *117*(12), 6330–6338.

Fougeron, N., Rohan, P.-Y., Haering, D., Rose, J.-L., Bonnet, X., & Pillet, H. (2020). Combining freehand ultrasound-based indentation and inverse finite element modelling for the identification of hyperelastic material properties of thigh soft tissues. *Journal of Biomechanical Engineering*, *142*(9), 091004.

Friedl, P., & Gilmour, D. (2009). Collective cell migration in morphogenesis, regeneration and cancer. *Nature Reviews. Molecular Cell Biology*, *10*(7), 445–457.

Gallinato, O., Ohta, M., Poignard, C., & Suzuki, T. (2017). Free boundary problem for cell protrusion formations: Theoretical and numerical aspects. *Journal of Mathematical Biology*, *75*(2), 263–307.

Ganesh, T., Laughrey, L. E., Niroobakhsh, M., & Lara-Castillo, N. (2020). Multiscale finite element modeling of mechanical strains and fluid flow in osteocyte lacunocanalicular system. *Bone*, *137*, 115328.

Gardel, M. L., Shin, J. H., MacKintosh, F. C., Mahadevan, L., Matsudaira, P., & Weitz, D. A. (2004). Elastic behavior of cross-linked and bundled actin networks. *Science*, *304*(5675), 1301–1305.

Gomez, H., Bures, M., & Moure, A. (2019). A review on computational modelling of phase-transition problems. *Philosophical Transactions of the Royal Society A: Mathematical, Physical and Engineering Sciences*, *377*(2143), 20180203.

Griffith, B. E. (2020). *An adaptive and distributed-memory parallel implementation of the immersed boundary (IB) method*. https://github.com/IBAMR/IBAMR

Guckenberger, A., & Gekle, S. (2017). Theory and algorithms to compute Helfrich bending forces: A review. *Journal of Physics. Condensed Matter*, *29*(20), 203001.

Guyot, Y., Luyten, F. P., Schrooten, J., Papantoniou, I., & Geris, L. (2015). A three-dimensional computational fluid dynamics model of shear stress distribution during neotissue growth in a perfusion bioreactor. *Biotechnology and Bioengineering*, *112*(12), 2591–2600.

Guyot, Y., Papantoniou, I., Chai, Y. C., Van Bael, S., Schrooten, J., & Geris, L. (2014). A computational model for cell/ECM growth on 3d surfaces using the level set method: A bone tissue engineering case study. *Biomechanics and Modeling in Mechanobiology*, *13*(6), 1361–1371.

Guyot, Y., Papantoniou, I., Luyten, F. P., & Geris, L. (2016). Coupling curvature-dependent and shear stress-stimulated neotissue growth in dynamic bioreactor cultures: A 3D computational model of a complete scaffold. *Biomechanics and Modeling in Mechanobiology*, *15*(1), 169–180.

Hannabuss, J., Lera-Ramirez, M., Cade, N. I., Fourniol, F. J., Nédélec, F., & Surrey, T. (2019). Self-organization of minimal anaphase spindle midzone bundles. *Current Biology*, *29*(13), 2120–2130.e7.

Hannezo, E., & Heisenberg, C.-P. (2019). Mechanochemical feedback loops in development and disease. *Cell*, *178*(1), 12–25.

Hayashi, A., Yavas, A., McIntyre, C. A., Ho, Y.-J., Erakky, A., Wong, W., … Iacobuzio-Donahue, C. A. (2020). Genetic and clinical correlates of entosis in pancreatic ductal adenocarcinoma. *Modern Pathology*, *33*(9), 1822–1831.

Hecht, I., Kessler, D. A., & Levine, H. (2010). Transient localized patterns in noise-driven reaction-diffusion systems. *Physical Review Letters*, *104*(15), 158301.

Hecht, I., Skoge, M. L., Charest, P. G., Ben-Jacob, E., Firtel, R. A., Loomis, W. F., … Rappel, W.-J. (2011). Activated membrane patches guide chemotactic cell motility. *PLoS Computational Biology*, *7*(6), e1002044.

Heck, T., Vargas, D. A., Smeets, B., Ramon, H., Van Liedekerke, P., & Van Oosterwyck, H. (2020). The role of actin protrusion dynamics in cell migration through a degradable viscoelastic extracellular matrix: Insights from a computational model. *PLoS Computational Biology*, *16*(1), e1007250.

Helfrich, W. (1973). Elastic properties of lipid bilayers: Theory and possible experiments. *Zeitschrift für Naturforschung. Section C*, *28*(11), 693–703.

Herant, M., Heinrich, V., & Dembo, M. (2005). Mechanics of neutrophil phagocytosis: Behavior of the cortical tension. *Journal of Cell Science*, *118*(Pt 9), 1789–1797.

Herant, M., Heinrich, V., & Dembo, M. (2006). Mechanics of neutrophil phagocytosis: Experiments and quantitative models. *Journal of Cell Science*, *119*(Pt 9), 1903–1913.

Herant, M., Lee, C.-Y., Dembo, M., & Heinrich, V. (2011). Protrusive push versus enveloping embrace: Computational model of phagocytosis predicts key regulatory role of cytoskeletal membrane anchors. *PLoS Computational Biology*, *7*(1), e1001068.

Hou, J. C., Maas, S. A., Weiss, J. A., & Ateshian, G. A. (2018). Finite element formulation of multiphasic shell elements for cell mechanics analyses in FEBio. *Journal of Biomechanical Engineering*, *140*(12), 121009.

Iglesias, P. A., & Devreotes, P. N. (2008). Navigating through models of chemotaxis. *Current Opinion in Cell Biology*, *20*(1), 35–40.

Ii, K., Mashimo, K., Ozeki, M., Yamada, T. G., Hiroi, N., & Funahashi, A. (2019). Xitosbml: A modeling tool for creating spatial systems biology markup language models from microscopic images. *Frontiers in Genetics*, *10*, 1027.

Janmey, P. A., Fletcher, D. A., & Reinhart-King, C. A. (2020). Stiffness sensing by cells. *Physiological Reviews*, *100*(2), 695–724.

Katti, D. R., & Katti, K. S. (2017). Cancer cell mechanics with altered cytoskeletal behavior and substrate effects: A 3d finite element modeling study. *Journal of the Mechanical Behavior of Biomedical Materials*, *76*, 125–134.

Keating, S. M., Waltemath, D., König, M., Zhang, F., Dräger, A., Chaouiya, C., … SBML Level 3 Community members. (2020). SBML Level 3: An extensible format for the exchange and reuse of biological models. *Molecular Systems Biology*, *16*(8), e9110.

Kennaway, R., & Coen, E. (2019). Volumetric finite-element modelling of biological growth. *Open Biology*, *9*(5), 190057.

Kim, M.-C., Silberberg, Y. R., Abeyaratne, R., Kamm, R. D., & Asada, H. H. (2018). Computational modeling of three-dimensional ECM-rigidity sensing to guide directed cell migration. *Proceedings of the National Academy of Sciences of the United States of America*, *115*(3), E390–E399.

Kothari, P., Johnson, C., Sandone, C., Iglesias, P. A., & Robinson, D. N. (2019). How the mechanobiome drives cell behavior, viewed through the lens of control theory. *Journal of Cell Science*, *132*(17), jcs234476.

Kouwer, P. H. J., Koepf, M., Le Sage, V. A. A., Jaspers, M., van Buul, A. M., Eksteen-Akeroyd, Z. H., … Rowan, A. E. (2013). Responsive biomimetic networks from polyisocyanopeptide hydrogels. *Nature*, *493*(7434), 651–655.

Kulawiak, D. A., Camley, B. A., & Rappel, W.-J. (2016). Modeling contact inhibition of locomotion of colliding cells migrating on micropatterned substrates. *PLoS Computational Biology*, *12*(12), e1005239.

Langtangen, H. P. (2012). A FEniCS tutorial. In A. Logg, K.-A. Mardal, & G. Wells (Eds.), *Automated solution of differential equations by the finite element method: The FEniCS book* (pp. 1–73). Berlin: Springer.

Lee, S. (2018). Mathematical model of contractile ring-driven cytokinesis in a three-dimensional domain. *Bulletin of Mathematical Biology*, *80* (3), 583–597.

Levchenko, A., & Iglesias, P. A. (2002). Models of eukaryotic gradient sensing: Application to chemotaxis of amoebae and neutrophils. *Biophysical Journal*, *82*(1 Pt 1), 50–63.

Li, Y., & Kim, J. (2016). Three-dimensional simulations of the cell growth and cytokinesis using the immersed boundary method. *Mathematical Biosciences*, *271*, 118–127.

Lo, C. M., Wang, H. B., Dembo, M., & Wang, Y. L. (2000). Cell movement is guided by the rigidity of the substrate. *Biophysical Journal*, *79* (1), 144–152.

Löber, J., Ziebert, F., & Aranson, I. S. (2015). Collisions of deformable cells lead to collective migration. *Scientific Reports*, *5*, 9172.

Ma, L., Janetopoulos, C., Yang, L., Devreotes, P. N., & Iglesias, P. A. (2004). Two complementary, local excitation, global inhibition mechanisms acting in parallel can explain the chemoattractant-induced regulation of pi(3,4,5)p3 response in dictyostelium cells. *Biophysical Journal*, *87*(6), 3764–3774.

Maas, S. A., Ellis, B. J., Ateshian, G. A., & Weiss, J. A. (2012). FEBio: Finite elements for biomechanics. *Journal of Biomechanical Engineering*, *134*(1), 011005.

Maas, S. A., LaBelle, S. A., Ateshian, G. A., & Weiss, J. A. (2018). A plugin framework for extending the simulation capabilities of FEBio. *Biophysical Journal*, *115*(9), 1630–1637.

Mackenzie, J. A., Nolan, M., Rowlatt, C. F., & Insall, R. H. (2019). An adaptive moving mesh method for forced curve shortening flow. *SIAM Journal on Scientific Computing*, *41*(2), A1170–A1200.

Marzban, B., Kang, J., Li, N., Sun, Y., & Yuan, H. (2019). A contraction–reaction–diffusion model: Integrating biomechanics and biochemistry in cell migration. *Extreme Mechanics Letters*, *32*, 100566.

Meinhardt, H. (1999). Orientation of chemotactic cells and growth cones: Models and mechanisms. *Journal of Cell Science*, *112*, 2867–2874.

Meyers, J., Craig, J., & Odde, D. J. (2006). Potential for control of signaling pathways via cell size and shape. *Current Biology*, *16*(17), 1685–1693.

Miao, Y., Bhattacharya, S., Banerjee, T., Abubaker-Sharif, B., Long, Y., Inoue, T., ... Devreotes, P. N. (2019). Wave patterns organize cellular protrusions and control cortical dynamics. *Molecular Systems Biology*, *15*(3), e8585.

Miao, Y., Bhattacharya, S., Edwards, M., Cai, H., Inoue, T., Iglesias, P. A., & Devreotes, P. N. (2017). Altering the threshold of an excitable signal transduction network changes cell migratory modes. *Nature Cell Biology*, *19*(4), 329–340.

Mietke, A., Jülicher, F., & Sbalzarini, I. F. (2019). Self-organized shape dynamics of active surfaces. *Proceedings of the National Academy of Sciences of the United States of America*, *116*(1), 29–34.

Mihai, L. A., & Goriely, A. (2017). How to characterize a nonlinear elastic material? A review on nonlinear constitutive parameters in isotropic finite elasticity. *Proceedings of the Royal Society A: Mathematical, Physical and Engineering Sciences*, *473*(2207), 20170607.

Minc, N., Burgess, D., & Chang, F. (2011). Influence of cell geometry on division-plane positioning. *Cell*, *144*(3), 414–426.

Mirams, G. R., Arthurs, C. J., Bernabeu, M. O., Bordas, R., Cooper, J., Corrias, A., ... Gavaghan, D. J. (2013). Chaste: An open source C++ library for computational physiology and biology. *PLoS Computational Biology*, *9*(3), e1002970.

Mitchell, I. M. (2008). The flexible, extensible and efficient toolbox of level set methods. *Journal of Scientific Computing*, *35*(2), 300–329.

Mogilner, A., & Manhart, A. (2016). Agent-based modeling: Case study in cleavage furrow models. *Molecular Biology of the Cell*, *27*(22), 3379–3384.

Mohammadi, H., & Sahai, E. (2018). Mechanisms and impact of altered tumour mechanics. *Nature Cell Biology*, *20*(7), 766–774.

Molina, J. J., & Yamamoto, R. (2019). Modeling the mechanosensitivity of fast-crawling cells on cyclically stretched substrates. *Soft Matter*, *15*(4), 683–698.

Moure, A., & Gomez, H. (2018). Three-dimensional simulation of obstacle-mediated chemotaxis. *Biomechanics and Modeling in Mechanobiology*, *17*(5), 1243–1268.

Moure, A., & Gomez, H. (2019). Phase-field modeling of individual and collective cell migration. *Archives of Computational Methods in Engineering*. https://doi.org/10.1007/s11831-019-09377-1

Moure, A., & Gomez, H. (2020a). Dual role of the nucleus in cell migration on planar substrates. *Biomechanics and Modeling in Mechanobiology*, *19*, 1491–1508.

Moure, A., & Gomez, H. (2020b). Influence of myosin activity and mechanical impact on keratocyte polarization. *Soft Matter*, *16*(22), 5177–5194.

Mukherjee, S., Nazemi, M., Jonkers, I., & Geris, L. (2020). Use of computational modeling to study joint degeneration: A review. *Frontiers in Bioengineering and Biotechnology*, *8*, 93.

Müller, R., & Rüegsegger, P. (1995). Three-dimensional finite element modelling of non-invasively assessed trabecular bone structures. *Medical Engineering & Physics*, *17*(2), 126–133.

Najem, S., & Grant, M. (2016). Phase-field model for collective cell migration. *Physical Review E*, *93*(5), 052405.

Nakamura, M., Bessho, S., & Wada, S. (2013). Spring-network-based model of a red blood cell for simulating mesoscopic blood flow. *International Journal of Numerical Methods in Biomedical Engineering*, *29*(1), 114–128.

Neilson, M. P., Mackenzie, J. A., Webb, S. D., & Insall, R. H. (2010). Use of the parameterised finite element method to robustly and efficiently evolve the edge of a moving cell. *Integrative Biology (Cambridge)*, *2*(11–12), 687–695.

Neilson, M. P., Veltman, D. M., van Haastert, P. J. M., Webb, S. D., Mackenzie, J. A., & Insall, R. H. (2011). Chemotaxis: A feedback-based computational model robustly predicts multiple aspects of real cell behaviour. *PLoS Biology*, *9*(5), e1000618.

Nguyen, A. V., Nyberg, K. D., Scott, M. B., Welsh, A. M., Nguyen, A. H., Wu, N., ... Rowat, A. C. (2016). Stiffness of pancreatic cancer cells is associated with increased invasive potential. *Integrative Biology (Cambridge)*, *8*(12), 1232–1245.

Nguyen, L. T. S., & Robinson, D. N. (2020). The unusual suspects in cytokinesis: Fitting the pieces together. *Frontiers in Cell and Development Biology*, *8*, 441.

Nickaeen, M., Novak, I. L., Pulford, S., Rumack, A., Brandon, J., Slepchenko, B. M., & Mogilner, A. (2017). A free-boundary model of a motile cell explains turning behavior. *PLoS Computational Biology*, *13*(11), e1005862.

Niculescu, I., Textor, J., & de Boer, R. J. (2015). Crawling and gliding: A computational model for shape-driven cell migration. *PLoS Computational Biology*, *11*(10), e1004280.

Nishimura, S. I., Ueda, M., & Sasai, M. (2009). Cortical factor feedback model for cellular locomotion and cytofission. *PLoS Computational Biology*, *5*(3), e1000310.

Nonomura, M. (2012). Study on multicellular systems using a phase field model. *PLoS One*, *7*(4), e33501.

Oakes, P. W., Bidone, T. C., Beckham, Y., Skeeters, A. V., Ramirez-San Juan, G. R., Winter, S. P., ... Gardel, M. L. (2018). Lamellipodium is a myosin-independent mechanosensor. *Proceedings of the National Academy of Sciences of the United States of America*, *115*(11), 2646–2651.

Osher, S., & Fedkiw, R. P. (2003). Level set methods and dynamic implicit surfaces. In *Applied mathematical sciences* (Vol. 153). New York: Springer.

Osher, S., & Sethian, J. A. (1988). Fronts propagating with curvature-dependent speed: Algorithms based on Hamilton–Jacobi formulations. *Journal of Computational Physics*, *79*(1), 12–49.

Overholtzer, M., Mailleux, A. A., Mouneimne, G., Normand, G., Schnitt, S. J., King, R. W., ... Brugge, J. S. (2007). A nonapoptotic cell death process, entosis, that occurs by cell-in-cell invasion. *Cell*, *131*(5), 966–979.

Parent, C. A., & Devreotes, P. N. (1999). A cell's sense of direction. *Science*, *284*(5415), 765–770.

Peskin, C. S. (1972). Flow patterns around heart valves: A numerical method. *Journal of Computational Physics*, *10*(2), 252–271.

Peskin, C. S. (2002). The immersed boundary method. *Acta Numerica*, *11*, 479–517.

Poirier, C. C., Ng, W. P., Robinson, D. N., & Iglesias, P. A. (2012). Deconvolution of the cellular force-generating subsystems that govern cytokinesis furrow ingression. *PLoS Computational Biology*, *8*(4), e1002467.

Pollard, T. D., & O'Shaughnessy, B. (2019). Molecular mechanism of cytokinesis. *Annual Review of Biochemistry*, *88*, 661–689.

Pons, J.-P., Hermosillo, G., Keriven, R., & Faugeras, O. (2006). Maintaining the point correspondence in the level set framework. *Journal of Computational Physics*, *220*(1), 339–354.

Rangamani, P., Lipshtat, A., Azeloglu, E. U., Calizo, R. C., Hu, M., Ghassemi, S., ... Iyengar, R. (2013). Decoding information in cell shape. *Cell*, *154*(6), 1356–1369.

Rappel, W.-J., & Edelstein-Keshet, L. (2017). Mechanisms of cell polarization. *Current Opinion in Systems Biology*, *3*, 43–53.

Reichl, E. M., Ren, Y., Morphew, M. K., Delannoy, M., Effler, J. C., Girard, K. D., ... Robinson, D. N. (2008). Interactions between myosin and actin crosslinkers control cytokinesis contractility dynamics and mechanics. *Current Biology*, *18*(7), 471–480.

Remmerbach, T. W., Wottawah, F., Dietrich, J., Lincoln, B., Wittekind, C., & Guck, J. (2009). Oral cancer diagnosis by mechanical phenotyping. *Cancer Research*, *69*(5), 1728–1732.

Rens, E. G., & Edelstein-Keshet, L. (2019). From energy to cellular forces in the cellular Potts model: An algorithmic approach. *PLoS Computational Biology*, *15*(12), e1007459.

Resasco, D. C., Gao, F., Morgan, F., Novak, I. L., Schaff, J. C., & Slepchenko, B. M. (2012). Virtual cell: Computational tools for modeling in cell biology. *WIREs: Systems Biology and Medicine*, *4*(2), 129–140.

Robinson, D. N., & Iglesias, P. A. (2012). Bringing the physical sciences into your cell biology research. *Molecular Biology of the Cell*, *23*(21), 4167–4170.

Roca-Cusachs, P., Sunyer, R., & Trepat, X. (2013). Mechanical guidance of cell migration: Lessons from chemotaxis. *Current Opinion in Cell Biology*, *25*(5), 543–549.

Rodrigues, M., Kosaric, N., Bonham, C. A., & Gurtner, G. C. (2019). Wound healing: A cellular perspective. *Physiological Reviews*, *99*(1), 665–706.

Rubinstein, B., Fournier, M. F., Jacobson, K., Verkhovsky, A. B., & Mogilner, A. (2009). Actin-myosin viscoelastic flow in the keratocyte lamellipod. *Biophysical Journal*, *97*(7), 1853–1863.

Satulovsky, J., Lui, R., & Wang, Y.-L. (2008). Exploring the control circuit of cell migration by mathematical modeling. *Biophysical Journal*, *94*(9), 3671–3683.

Schaff, J. C., Gao, F., Li, Y., Novak, I. L., & Slepchenko, B. M. (2016). Numerical approach to spatial deterministic-stochastic models arising in cell biology. *PLoS Computational Biology*, *12*(12), e1005236.

Schneider, I. C., & Haugh, J. M. (2005). Quantitative elucidation of a distinct spatial gradient-sensing mechanism in fibroblasts. *The Journal of Cell Biology*, *171*(5), 883–892.

Sethian, J. A. (1999). *Level set methods and fast marching methods: Evolving interfaces in computational geometry, fluid mechanics, computer vision, and materials science* (2nd ed.). Cambridge, England: Cambridge University Press.

Shao, D., Levine, H., & Rappel, W.-J. (2012). Coupling actin flow, adhesion, and morphology in a computational cell motility model. *Proceedings of the National Academy of Sciences of the United States of America*, *109*(18), 6851–6856.

Shao, D., Rappel, W.-J., & Levine, H. (2010). Computational model for cell morphodynamics. *Physical Review Letters*, *105*(10), 108104.

Shi, C., Huang, C.-H., Devreotes, P. N., & Iglesias, P. A. (2013). Interaction of motility, directional sensing, and polarity modules recreates the behaviors of chemotaxing cells. *PLoS Computational Biology*, *9*(7), e1003122.

Shlomovitz, R., & Gov, N. S. (2008). Physical model of contractile ring initiation in dividing cells. *Biophysical Journal*, *94*(4), 1155–1168.

Storm, C., Pastore, J. J., MacKintosh, F. C., Lubensky, T. C., & Janmey, P. A. (2005). Nonlinear elasticity in biological gels. *Nature*, *435*(7039), 191–194.

Strychalski, W., Adalsteinsson, D., & Elston, T. C. (2010). Simulating biochemical signaling networks in complex moving geometries. *SIAM Journal on Scientific Computing*, *32*(5), 3039–3070.

Sun, Q., Luo, T., Ren, Y., Florey, O., Shirasawa, S., Sasazuki, T., ... Overholtzer, M. (2014). Competition between human cells by entosis. *Cell Research*, *24*(11), 1299–1310.

Surcel, A., & Robinson, D. N. (2019). Meddling with myosin's mechanobiology in cancer. *Proceedings of the National Academy of Sciences of the United States of America*, *116*(31), 15322–15323.

Surcel, A., Schiffhauer, E. S., Thomas, D. G., Zhu, Q., DiNapoli, K. T., Herbig, M., ... Robinson, D. N. (2019). Targeting mechanoresponsive proteins in pancreatic cancer: 4-Hydroxyacetophenone blocks dissemination and invasion by activating MYH14. *Cancer Research*, *79*(18), 4665–4678.

Swaminathan, V., Mythreye, K., O'Brien, E. T., Berchuck, A., Blobe, G. C., & Superfine, R. (2011). Mechanical stiffness grades metastatic potential in patient tumor cells and in cancer cell lines. *Cancer Research*, *71*(15), 5075–5080.

Swat, M. H., Thomas, G. L., Belmonte, J. M., Shirinifard, A., Hmeljak, D., & Glazier, J. A. (2012). Multi-scale modeling of tissues using CompuCell3D. *Methods in Cell Biology*, *110*, 325–366.

Tang, G., Galluzzi, M., Zhang, B., Shen, Y.-L., & Stadler, F. J. (2019). Biomechanical heterogeneity of living cells: Comparison between atomic force microscopy and finite element simulation. *Langmuir*, *35*(23), 7578–7587.

Tao, K., Wang, J., Kuang, X., Wang, W., Liu, F., & Zhang, L. (2020). Tuning cell motility via cell tension with a mechanochemical cell migration model. *Biophysical Journal*, *118*(12), 2894–2904.

Teo, S.-K., Goryachev, A. B., Parker, K. H., & Chiam, K.-H. (2010). Cellular deformation and intracellular stress propagation during optical stretching. *Physical Review E: Statistical, Nonlinear, and Soft Matter Physics*, *81*(5 Pt 1), 051924.

Thompson, D. W. (1917). *On growth and form*. Cambridge: Cambridge University Press.

Thüroff, F., Goychuk, A., Reiter, M., & Frey, E. (2019). Bridging the gap between single-cell migration and collective dynamics. *eLife*, *8*, e46842.

Tollis, S., Dart, A. E., Tzircotis, G., & Endres, R. G. (2010). The zipper mechanism in phagocytosis: Energetic requirements and variability in phagocytic cup shape. *BMC Systems Biology*, *4*, 149.

Ujihara, Y., Nakamura, M., Miyazaki, H., & Wada, S. (2010). Proposed spring network cell model based on a minimum energy concept. *Annals of Biomedical Engineering*, *38*(4), 1530–1538.

Valero, C., Navarro, B., Navajas, D., & García-Aznar, J. M. (2016). Finite element simulation for the mechanical characterization of soft biological materials by atomic force microscopy. *Journal of the Mechanical Behavior of Biomedical Materials*, *62*, 222–235.

Vanderlei, B., Feng, J. J., & Edelstein-Keshet, L. (2011). A computational model of cell polarization and motility coupling mechanics and biochemistry. *Multiscale Modeling and Simulation*, *9*(4), 1420–1443.

Varennes, J., Han, B., & Mugler, A. (2016). Collective chemotaxis through noisy multicellular gradient sensing. *Biophysical Journal*, *111*(3), 640–649.

Vavylonis, D., Wu, J.-Q., Hao, S., O'Shaughnessy, B., & Pollard, T. D. (2008). Assembly mechanism of the contractile ring for cytokinesis by fission yeast. *Science*, *319*(5859), 97–100.

Walker, C., Mojares, E., & Del Río Hernández, A. (2018). Role of extracellular matrix in development and cancer progression. *International Journal of Molecular Sciences*, *19*(10), 3028.

Wolgemuth, C. W., & Zajac, M. (2010). The moving boundary node method: A level set-based, finite volume algorithm with applications to cell motility. *Journal of Computational Physics*, *229*(19), 7287–7308.

Xin, Y., Chen, X., Tang, X., Li, K., Yang, M., Tai, W. C.-S., ... Tan, Y. (2019). Mechanics and actomyosin-dependent survival/chemoresistance of suspended tumor cells in shear flow. *Biophysical Journal*, *116*(10), 1803–1814.

Xiong, Y., Kabacoff, C., Franca-Koh, J., Devreotes, P. N., Robinson, D. N., & Iglesias, P. A. (2010). Automated characterization of cell shape changes during amoeboid motility by skeletonization. *BMC Systems Biology*, *4*, 33.

Yang, L., Effler, J. C., Kutscher, B. L., Sullivan, S. E., Robinson, D. N., & Iglesias, P. A. (2008). Modeling cellular deformations using the level set formalism. *BMC Systems Biology*, *2*, 68.

Yang, Y., Jolly, M. K., & Levine, H. (2019). Computational modeling of collective cell migration: Mechanical and biochemical aspects. *Advances in Experimental Medicine and Biology*, *1146*, 1–11.

Yang, Y., & Levine, H. (2018). Role of the supracellular actomyosin cable during epithelial wound healing. *Soft Matter*, *14*, 4866–4873.

Zhan, H., Bhattacharya, S., Cai, H., Iglesias, P. A., Huang, C.-H., & Devreotes, P. N. (2020). An excitable Ras/PI3K/ERK signaling network controls migration and oncogenic transformation in epithelial cells. *Developmental Cell*, *54*(5), 608–623.e5.

Zhang, W., & Robinson, D. N. (2005). Balance of actively generated contractile and resistive forces controls cytokinesis dynamics. *Proceedings of the National Academy of Sciences of the United States of America*, *102*(20), 7186–7191.

Zhang, Z., Rosakis, P., Hou, T. Y., & Ravichandran, G. (2020). A minimal mechanosensing model predicts keratocyte evolution on flexible substrates. *Journal of the Royal Society Interface*, *17*(166), 20200175.

Zhao, H.-K., Chan, T., Merriman, B., & Osher, S. (1996). A variational level set approach to multiphase motion. *Journal of Computational Physics*, *127*(1), 179–195.

Zhao, J., & Wang, Q. (2016a). A 3D multi-phase hydrodynamic model for cytokinesis of eukaryotic cells. *Communications in Computational Physics*, *19*(3), 663–681.

Zhao, J., & Wang, Q. (2016b). Modeling cytokinesis of eukaryotic cells driven by the actomyosin contractile ring. *International Journal of Numerical Methods in Biomedical Engineering*, *32*(12), e02774.

Zhou, E. H., Xu, F., Quek, S. T., & Lim, C. T. (2012). A power-law rheology-based finite element model for single cell deformation. *Biomechanics and Modeling in Mechanobiology*, *11*(7), 1075–1084.

Zhu, J., & Mogilner, A. (2016). Comparison of cell migration mechanical strategies in three-dimensional matrices: A computational study. *Interface Focus*, *6*(5), 20160040.

Ziebert, F., & Aranson, I. S. (2013). Effects of adhesion dynamics and substrate compliance on the shape and motility of crawling cells. *PLoS One*, *8*(5), e64511.

Zienkiewicz, O. C., & Taylor, R. L. (2000). *The finite element method* (5th ed.). Butterworth-Heinemann: Oxford.

Zimmermann, J., Camley, B. A., Rappel, W.-J., & Levine, H. (2016). Contact inhibition of locomotion determines cell–cell and cell–substrate forces in tissues. *Proceedings of the National Academy of Sciences of the United States of America*, *113*(10), 2660–2665.

Zmurchok, C., & Holmes, W. R. (2020). Simple Rho GTPase dynamics generate a complex regulatory landscape associated with cell shape. *Biophysical Journal*, *118*(6), 1438–1454.

How to cite this article: DiNapoli KT, Robinson DN, Iglesias PA. Tools for computational analysis of moving boundary problems in cellular mechanobiology. *WIREs Mech Dis*. 2020;e1514. https://doi.org/10.1002/wsbm.1514